Jorge Antonio Gonçalves Attie

Blockade and Antiblockade effects with near-ground state neutral atoms

São Carlos

2022

Jorge Antonio Gonçalves Attie

Blockade and Antiblockade effects with near-ground state neutral atoms

Master thesis presented to the Universidade Federal de São Carlos, Departamento de Física, as a necessary requirement to obtain the master's degree in Physics

Universidade Federal de São Carlos

Departamento de Física

Advisor: Romain Pierre Marcel Bachelard

Co-supervisor: André Cidrim Santos

São Carlos

2022

Talvez *agridoce* seja a melhor palavra para descrever o que foram os dois anos ao longo dos quais esse trabalho foi desenvolvido, afinal apesar de ter alcançado objetivos que há muito tempo almejava, foram anos difíceis em todos os sentidos. Mas, como já colocou Guimarães Rosa: *O correr da vida embrulha tudo. A vida é assim: esquenta e esfria, aperta e daí afrouxa, sossega e depois desinquieta. O que ela quer da gente é coragem.* Com isso, minha dedicatória não poderia ser diferente: à minha mãe Gilce e meu pai Antonio pelo constante e incansável suporte, e a minha filha Lorena por ser o sentido de minha caminhada e o combustível para absolutamente tudo o que faço.

Acknowledgements

I would like to thank my parents, Gilce and Antonio, by the constant support and incentive to my studies and career, to my friends which even physically distant in these last years remained presented in my life as a safe refuge. I would like to thank also my daughter, which even without knowing relieves me of all my worries whenever I see her smile.

I am very grateful to my advisor Romain to accepting me as a student although I was completely inexperienced in the area, to the patience, to the teachings and especially to show me a way of doing science that was totally new to me.

I am immensely grateful to my co-advisor André by everything which he taught me (what was a lot!) and by the huge patience, weak by weak, in teaching me, repeat and to insist until I have achieved what he wanted to pass on to me. I am equally grateful to Alan, by the availability and to help me in crucial points of this work.

Moreover, I am deeply grateful to all my professors and colleagues which in some way enriched my master's degree.

The study presented on this dissertation was financed by CAPES and all the support and structure was offered by the Federal University of São Carlos.

Abstract

In this work we study the photon blockade and antiblockade effects in a system of neutral atoms with a two-level structure, in the limit where induced dipole-dipole interactions mediated by light are relevant. Such system is an interesting alternative to cold gases platforms with Rydberg atoms, with applications in quantum optics and quantum information protocols. For an ensemble of few atoms driven by a laser field, we monitor the photon statistics and the population dynamics of the excited states, identifying the regime of parameters under which blockade or antiblockade is achieved. Furthermore we study the correlations, non-classicality and entanglement of the emitted photons through the photon-photon correlations function and the Cauchy-Schwarz and Bell's inequalities, with the aim of obtaining a source of pairs of photons strongly correlated and entangled.

Keywords: Blockade Effect, Antiblockade Effect.

Resumo

Nós estudamos neste trabalho os efeitos de bloqueio e antibloqueio de fótons em um sistema de átomos neutros com uma estrutura de dois níveis, no limite no qual as interações dipolo-dipolo mediadas pela luz são relevantes. Tal sistema mostra-se uma alternativa interessante à plataformas de gases frios com átomos de Rydberg, possuindo aplicações em óptica quântica e em protocolos de informação quântica. Para uma conjunto de alguns átomos interagindo com um campo de radiação externo, nós monitoramos a estatística da luz e a dinâmica populacional dos estados de excitações, identificando o regime de parâmetros sob os quais os efeitos de bloqueio e antibloqueio se manifestam. Além disso, nós estudamos as correlações, não-classicalidade e emaranhamento dos fótons emitidos através das funções de correlação fóton-fóton e das desigualdades de Cauchy-Schwarz e de Bell, com o objetivo de obter uma fonte de pares de fótons fortemenete correlacionados e emaranhados.

Palavras-chave: Efeito de Bloqueio, Efeito de Antibloqueio

List of Figures

Contents

1 Introduction

The interaction between light and matter gives rise to a series of phenomena and applications in physics, ranging from the construction of optoelectronic devices [3] to the study of the composition of the universe [4]. In the case of neutral atoms interacting with an external radiation field, one can already observe the manifestation of various phenomena, such as the blockade and antiblockade effect. The blockade effect is a regime where multiple-excitation states are weakly populated and at most one excitation is energetically allowed in the system. Conversely, the antiblockade effect favors multiple-excitation states as compared to single-excitation ones. So, when the blockade (antiblockade) is achieved, it indicates that the system is more likely to emit single-photon (bundles of photons). As highlighted by Amthor et al. [5], it is of interest to achieve and control these effects for several applications: creation and manipulation of entangled states [6, 7, 8], quantum gates construction [9, 10], resonant energy transfer [11, 12], many-body effects in an ultracold atomic gas [13], quantum mechanical transport phenomena [14], and for the study of long-range molecules [15, 16].

Most works about the blockade and antiblockade effect were done considering an ensemble of Rydberg atoms[1] in free-space since they are propitious to establish strong interactions due to their large principal quantum number [18]. However, such atoms have some drawbacks, such as their high vulnerability to the presence of electric and magnetic fields — it is a motivation to search for alternative platforms where such effects can be emulated. The blockade effect was observed for an ensemble of two-level neutral atoms near ground state in the subwavelength regime by Cidrim et al. [2]. In our work, we use the same atomic model to explore the blockade and antiblockade effects to determine under which conditions a light-atom system exhibits the inhibition or facilitation of multiple excitations. This would allow studying regimes where pairs of correlated photons are favored, considering a frequency-filtering of the emitted photons. From a theoretical point of view, the so-called sensor method [19, 20, 21] was recently introduced: a theoretical proposal that allows us to extract the correlations of photons emitted by a system of interest (e.g. an atomic cloud) by weakly coupling this system to sensors (which can be frequency-tunable two-level systems). Using this method, it is possible to reduce the computational effort necessary to calculate high-order photon-photon correlations, since instead of obtaining the solutions of Heisenberg equations and expressing their correlations in terms of the system operators, the intensity-intensity correlations are computed between sensors directly [22, 23].

[1] Rydberg atoms: a class of atoms where the valence electron is in a state of high principal quantum number, which results in strong atom-atom interactions. Their large dimensions turn them easier to experimentally manipulate than other types of atoms [17].

The use of the sensor method to compute photon-photon correlations and their detailed characteristics has already been reported in a series of works in the field [19, 20, 22, 23, 24, 21]. We aim here to extend the study of this subject as follows: applying the sensor method using the vectorial model of light (typically the scalar model is used) for the description of the light-matter interaction in the blockade and antiblockade regime, so we can obtain information about the correlation, entanglement, and (non -)classical nature of the pairs of photons emission.

2 Theoretical Concepts

2.1 Quantization of the radiation field

To explore the photon blockade or antiblockade, it is necessary to consider the quantization of the electromagnetic field radiated by atoms. To proceed with the quantization of the field, we first define a set of spatial modes described by the wavevector $\vec{k}$, wherein each mode has two polarizations defined by the unit vector $\hat{e}_{\vec{k},\lambda}$ (here λ indicates the direction of polarization) and represents a quantum harmonic oscillator with energy levels separated by the quantity $\hbar\omega_{\vec{k}}$ ($\omega_{\vec{k}} = c|\vec{k}|$). In this representation, a photon in mode $\vec{k}$ corresponds to the excitation of this mode. Photons are added or removed by, respectively, the creation operator $\hat{a}^{\dagger}_{\vec{k},\lambda}|n_{\vec{k},\lambda}\rangle = \sqrt{n_{\vec{k},\lambda}+1}\,|n_{\vec{k},\lambda}+1\rangle$ or the annihilation operator $\hat{a}_{\vec{k},\lambda}|n_{\vec{k},\lambda}\rangle = \sqrt{n_{\vec{k},\lambda}}\,|n_{\vec{k},\lambda}-1\rangle$ applied over the state $|n_{\vec{k},\lambda}\rangle$. In these equations, $n_{\vec{k},\lambda}$ represents the number of photons in mode $\vec{k}$ and labels the eigenstates (also known as Fock states) of the number operator $\hat{n}_{\mathrm{obs}\vec{k},\lambda} = \hat{a}^{\dagger}_{\vec{k},\lambda}\hat{a}_{\vec{k},\lambda}$. Therefore, the electric field at a position $\vec{r}$ and instant t can be expressed as follows [1]:

$$\hat{E}(\vec{r},t) = i\sum_{\vec{k},\lambda}\sqrt{\frac{\hbar\omega_{\vec{k}}}{2\epsilon_0 V}}\hat{e}_{\vec{k},\lambda}\left[\hat{a}_{\vec{k},\lambda}(t)e^{-i\omega_{\vec{k}}t+i\vec{k}\cdot\vec{r}} - \hat{a}^{\dagger}_{\vec{k},\lambda}(t)e^{i\omega_{\vec{k}}t-i\vec{k}\cdot\vec{r}}\right], \tag{2.1}$$

where ϵ_0 is the vacuum per the environment is the so-called quantization volume. Equation (2.1) can be shortly expressed as $\hat{E}(\vec{r},t) = \hat{E}^{+}(\vec{r},t) + \hat{E}^{-}(\vec{r},t)$, where:

$$\begin{aligned}\hat{E}^{+}(\vec{r},t) &= i\sum_{\vec{k},\lambda}\sqrt{\frac{\hbar\omega_{\vec{k}}}{2\epsilon_0 V}}\hat{e}_{\vec{k},\lambda}\hat{a}_{\vec{k},\lambda}(t)e^{-i\omega_{\vec{k}}t+i\vec{k}\cdot\vec{r}},\\ \hat{E}^{-}(\vec{r},t) &= i\sum_{\vec{k},\lambda}\sqrt{\frac{\hbar\omega_{\vec{k}}}{2\epsilon_0 V}}\hat{e}_{\vec{k},\lambda}\hat{a}^{\dagger}_{\vec{k},\lambda}(t)e^{i\omega_{\vec{k}}t-i\vec{k}\cdot\vec{r}}.\end{aligned} \tag{2.2}$$

Thus $\hat{E}^{+}(\vec{r},t)$ is written as a function of annihilation operators and $\hat{E}^{-}(\vec{r},t)$ as a function of creation operators, satisfy $[\hat{E}^{+}(\vec{r},t)]^{\dagger} = \hat{E}^{-}(\vec{r},t)$.

The intensity of the electric field measured by a detector is related to the expectation value $\langle\hat{I}(\vec{r},t)\rangle$, where $\hat{I}(\vec{r},t) = \hat{E}^{-}(\vec{r},t)\hat{E}^{+}(\vec{r},t)$. To differentiate a quantum from a classical field, it is typically not enough to monitor its average electric field or its intensity, one must also consider intensity-intensity correlations. In particular, the non-classical nature of light can be further investigated using temporal and spatial correlations of the field, as we shall see next.

2.2 Photon Statistics

Let us first discuss photon statistics by introducing the concept of the *degree of second-order coherence*, which is a way of quantifying the correlations between photons at different positions and instants of time [25]. Typically, a detector uses the photoelectric effect to make local measurements of the field. The photoelectric effect is a phenomenon in which we have the emission of electrons due to the interaction between electromagnetic radiation and matter, the electrons emitted in this way are called *photon-electrons* [26]. Taking the example of an atom in the ground state and positioned at $\vec{r}$ in the radiation field, the process of photo-electron emission happens through the following mechanism: an electron (usually the farthest from the nucleus) absorbs a photon from the field, being excited and detaching from the atom — if the photon's energy is sufficient for this [26]. However, when the electron jumps back to its original state, the absorbed photon is emitted back into the field and, because of this, a photon-electron can be indirectly measured by the detection of the emitted photons. So, the probability of a photon be absorbed by an atom in $\vec{r}$ between the time instants t and $t + dt$ is proportional to the photodetector count rate $w_1(\vec{r}, t)$, which can be expressed by:

$$w_1(\vec{r}, t) = |\langle f|\hat{E}^+(\vec{r}, t)|i\rangle|^2, \tag{2.3}$$

where $|i\rangle$ is the initial state of the field (before the detection process) and $|f\rangle$ is the final state of the field (after the detection process) [25].

For the joint count rate $w_2(\vec{r}_1, t_1, \vec{r}_2, t_2)$ of two photodetectors located at $\vec{r}_1$ and $\vec{r}_2$, the probability of observing a photoionization at $\vec{r_1}$ (between t_1 and $t_1 + dt_1$) and another at $\vec{r}_2$ (between t_2 and $t_2 + dt_2$), with $t_1 \leq t_2$, is given by:

$$w_2(\vec{r}_1, \vec{r}_2; t_1, t_2) = |\langle f|\hat{E}^+(\vec{r}_2, t_2)\hat{E}^+(\vec{r}_1, t_1)|i\rangle|^2. \tag{2.4}$$

From this expression, we can get:

$$w_2(\vec{r}_1, t_1; \vec{r}_2, t_2) = \langle i|\hat{E}^-(\vec{r}_2, t_2)\hat{E}^-(\vec{r}_1, t_1)|f\rangle \langle f|\hat{E}^+(\vec{r}_2, t_2)\hat{E}^+(\vec{r}_1, t_1)|i\rangle . \tag{2.5}$$

Since the final state of the field can be any, we can rewrite (2.5) taking into account all final states [25]

$$w_2(\vec{r}_1, t_1; \vec{r}_2, t_2) = \sum_f \langle i|\hat{E}^-(\vec{r}_2, t_2)\hat{E}^-(\vec{r}_1, t_1)|f\rangle \langle f|\hat{E}^+(\vec{r}_2, t_2)\hat{E}^+(\vec{r}_1, t_1)|i\rangle . \tag{2.6}$$

This expression can be reduced using the completeness relation $\sum_f |f\rangle \langle f| = 1$:

$$w_2(\vec{r}_1, t_1; \vec{r}_2, t_2) = \langle i|\hat{E}^-(\vec{r}_2, t_2)\hat{E}^-(\vec{r}_1, t_1)\hat{E}^+(\vec{r}_2, t_2)\hat{E}^+(\vec{r}_1, t_1)|i\rangle . \tag{2.7}$$

In practice, however, the initial state is usually not known precisely and it is necessary to resort to a statistical description, that is: taking the average over all possible

initial states set. Then, we obtain:

$$w_2(\vec{r}_1, t_1, \vec{r}_2, t_2) = \sum_i P_i \langle i|\hat{E}^-(\vec{r}_2, t_2)\hat{E}^-(\vec{r}_1, t_1)\hat{E}^+(\vec{r}_2, t_2)\hat{E}^+(\vec{r}_1, t_1)|i\rangle \,, \tag{2.8}$$

where P_i is the probability associated with the initial state $|i\rangle$, and the expectation value inside the sum can be rewritten in a more compact way: $\langle \hat{E}^-(\vec{r}_2, t_2)\hat{E}^-(\vec{r}_1, t_1)\hat{E}^+(\vec{r}_2, t_2)\hat{E}^+(\vec{r}_1, t_1)\rangle$, where the initial state is implied. This expectation value defines what is known as the second-order correlation function:

$$G^{(2)}(\vec{r}_1, \vec{r}_2; t_1, t_2) = \langle \hat{E}^-(\vec{r}_2, t_2)\hat{E}^-(\vec{r}_1, t_1)\hat{E}^+(\vec{r}_2, t_2)\hat{E}^+(\vec{r}_1, t_1)\rangle \,. \tag{2.9}$$

In this work, we deal with stationary fields, which implies that the correlation functions are invariant under temporal displacements, in a way that such functions are dependent on t_1 and t_2 only through the time difference $\tau = t_2 - t_1$ [25]. Furthermore, we also consider the scattered electric field in the far-field approximation, so: $\hat{E}^{\pm} \propto \sum_{i=1}^{N} e^{-ik\hat{n}\cdot\vec{r}_i}\sigma_i^{\mp}$, with $\hat{n}$ the direction of observation. Here $\sigma_i^{-/+}$ is the lowering/raising atomic operator and the correlation functions can be expressed only as a function of τ (the position dependence disappears due to the far-field consideration, and the dependence on the angle of observation $\hat{n}$ is kept implicit), which allow us to simplify Eq. (2.9) as follows:

$$G^{(2)}(\tau) = \lim_{t\to\infty} \langle \hat{E}^-(t)\hat{E}^-(t+\tau)\hat{E}^+(t+\tau)\hat{E}^+(t)\rangle \,, \tag{2.10}$$

where the limit $t \to \infty$ indicates the steady state of the atomic system [2]. By renormalizing the correlation function, we can define the degree of second-order coherence (also called photon-photon correlation function) as:

$$g^{(2)}(\tau) = \lim_{t\to\infty} \frac{\langle \hat{E}^-(t)\hat{E}^-(t+\tau)\hat{E}^+(t+\tau)\hat{E}^+(t)\rangle}{\langle \hat{E}^-(t)\hat{E}^+(t)\rangle^2}. \tag{2.11}$$

For a classical field, the degree of second-order coherence at $\tau = 0$ satisfies the inequality $g^{(2)}(0) \geq 1$. However for a quantum field we only have that $0 \leq g^{(2)}(0) \leq \infty$, so $g^{(2)}(0) < 1$ can be used as an indicator of a non-classical state of light [27]. For instance, for a Fock state $|n\rangle$, with n the exact number of photons in the state, which is a state with no classical analogue, $g^{(2)}(0) = 1 - \frac{1}{n}$ is always smaller than one. In particular, $g^{(2)}(0) = 0$ for a single photon, and the physical interpretation behind this result is the following: for a well-defined single-photon state, one cannot simultaneously observe two photons arriving at the same time. This effect is named *anti-bunching* and it is a characteristic of any source with $g^{(2)}(0) < 1$, indicating that photons arrive preferentially at the detectors separated by a finite time. Similarly, states with $g^{(2)}(0) > 1$ are associated with the opposite effect named *bunching*, for which it is more likely for photons to arrive together ("bunched") at the detectors [27].

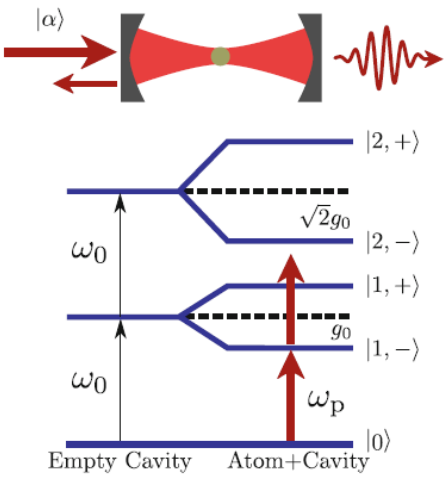

Figure 1 – Schematic of the photon blockade phenomenon. An atom inside the cavity causes the detuning of the cavity modes by $\pm\sqrt{n}g_0$ (g_0 is the coupling constant), preventing more than a single photon enters the cavity. Reference: [1]

2.3 The Blockade and Antiblockade Effect

Every mode of the quantized electric field behaves like a harmonic oscillator and an optical cavity is an interesting platform to investigate how emitters interact with a single mode of the field. In Fig. 1, we have the representation of the energy levels structure for two different situations: an empty cavity and a cavity with an atom trapped inside. We can see that for the empty cavity, there is a harmony between the energy levels — such structure is called *bare states*, and the transition energy between these states is ω_0. Placing an atom inside the cavity causes the cavity modes to be detuned from ω_0 by $\sqrt{n}g_0$ (g_0 is a coupling constant that quantifies the atom-cavity interaction, n is the photon number in the cavity mode), breaking the harmony between the energy levels— this new structure is called *dressed states*, being denoted by $|n,\pm\rangle$. As a consequence of this detuning, multiple-photon states become off resonant and only one photon can be inserted into the cavity at a time. This effect is an example of the photon blockade, which we discuss in more detail below.

Photon blockade was proposed for the first time by Imamoglu et al. in 1997 [28], receiving this name by analogy with the Coulomb blockade. In the latter case, small electronic devices behave as a turnstile system for current flow: electrons are transported through the system one at a time due to the reduced system size which prevents the insertion of a second electron by electrostatic repulsion. A similar phenomenon happens in several systems where light interacts with matter. The blockade effect acts now on the flow of photons: an effective and strong nonlinear interaction between the photons prevents the presence of two photons at a time in the system. The photon blockade effect was initially observed as a consequence of the strong effective photon-photon interactions inside a

confocal cavity with a low-density atomic medium [28]. Some years later, the observation of the photon blockade was reported in experiments that studied the photon statistics of the transmitted light in an optical cavity with one trapped atom in the strong coupling regime [29]. Following these observations of the photon blockade, the phenomenon was the focus of further theoretical and experimental investigations. For example, it was observed in a weakly driven optomechanical system under a strong coupling regime with a single photon [30], in a waveguide containing two atoms coupled via Rydberg interaction [31], and also investigated by Urban et al. [32] and Gaëtan et al. [33] the so-called *Rydberg Blockade*, where neutral atoms are excited to Rydberg states via dipole-dipole or van der Waals interaction.

Another platform in which the photon blockade was reported is an ensemble of two-level ground state neutral atoms with dipole-dipole interaction between them [2, 34]. In atomic systems, the photon blockade has been achieved using Rydberg states, describing atoms excited to a high-energy level, with a large principal quantum number [18]. Indeed, Rydberg systems are interesting platforms to achieve the blockade effect due to the strong interaction between the atoms, which can be much larger than other interactions for ground state atoms. Such interactions lead to a strong repulsion between two Rydberg atoms, turning the multi-excitation states non-resonant with a laser drive tuned to the Rydberg transition. However, although Rydberg physics is propitious to generating appreciable quantum correlations, it suffers from some drawbacks. Their large dipole moments make them extremely sensitive to surrounding electric and magnetic fields. This motivates the search for alternative atomic systems with similar effects.

A system of near-ground state, two-level neutral atoms [2] is different from the situation of Rydberg systems, whose dimensions are of the order of a few micrometers and which interact over even longer distances. Indeed, in the work of Cidrim et al. [2], subwavelength samples of atoms were considered to obtain strong interactions, motivated by the recent progress in the creation of subwavelength structures [35, 36, 37]. This allows for a blockade-like effect, similarly to Rydberg atoms, but with an important difference: the energy shifts occur for the single-excitation states and not in the highly excited states as in the case of Rydberg atoms. In the protocol proposed [2], a single-excitation collective state acquires an energy shift Δ_{SR} as a result of the induced dipole-dipole interactions. When these interactions are strong enough and a laser is set on resonance with a single-excitation collective state, the resulting large Δ_{SR} makes the two-excitation states off resonant, preventing their presence in the system. Then, the system holds only one excitation at a time, so only one photon is emitted at a time too, configuring the photon blockade. The corresponding energy levels for $N = 2$ Rydberg and ground state atoms are compared in Fig. 2.

There also exists the antiblockade effect, in which the multiple-excitation states

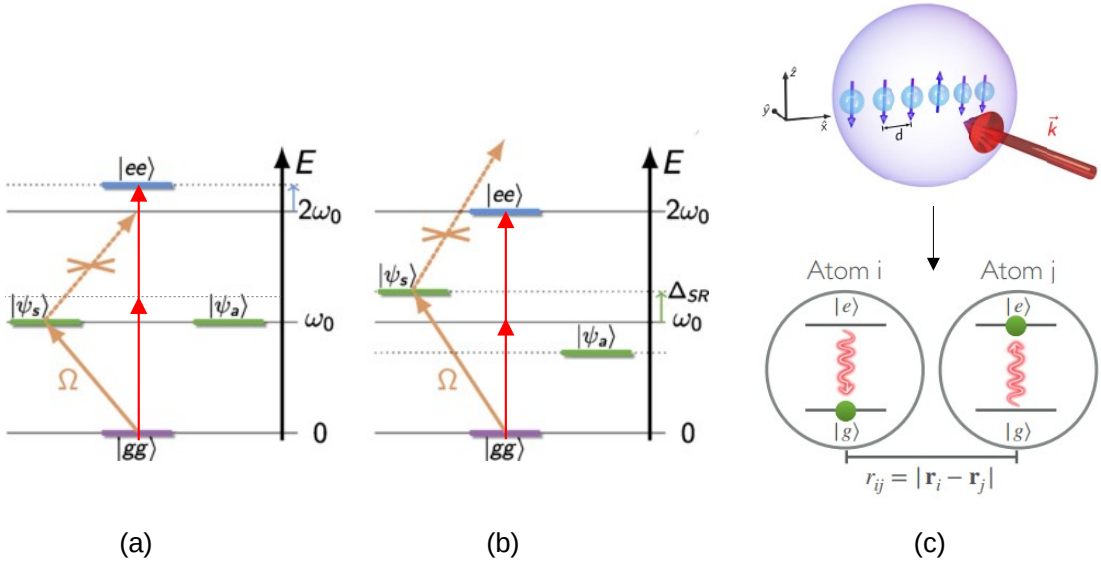

Figure 2 – The blockade (orange arrows) and antiblockade (red arrows) mechanism for a system with two atoms ($N = 2$). In **(a)** we present the Rydberg configuration where the energy shift occurs on the two-excitation states. In **(b)** we present the configuration of the system with strong induced dipole-dipole interactions, where the energy shift happens in the single-excitation states. **(c)** The atomic system considered in this work and its interaction with the radiation field: a linear chain of atoms regularly spaced and distributed along $\hat{x}$ is pumped by an incident laser along $\hat{y}$. Considering a many-atom system interacting via their induced dipoles, when a photon from the driving laser excites an atom i, a coherent interaction with another atom j is established: a virtual photon is exchanged back and forth between the interacting atoms, in a so-called "flip-flop"process. After a relaxation time (that also depends on the strength of the dipole-dipole interactions between the atoms), a real photon is emitted into the radiation field in the form of spontaneous emission. Furthermore, for an atomic ensemble with strong induced dipole-dipole interactions, one has that the symmetric and antisymmetric ($|\Psi_a\rangle$) single-excitation states are oppositely separated. So, for the incident laser to guide the atomic system to the symmetric state ($|\Psi_s\rangle$), its energy is detuned by Δ_{SR}. The purple shaded sphere around the atomic chain represents the blockade region. Reference: Adapted from [2]

.

are preferentially populated, see Fig. 2 (red arrows). The antiblockade was theoretically proposed by Ates et al. in 2007 [38] and its experimental observation was reported by Amthor et al. in 2010 [39]. This phenomenon has been used to study motional effects [40], dissipative dynamics-based entangled state production [7], and construction of quantum gates [10], for example.

In this work, we explore the antiblockade effect for a system composed of ground state neutral atoms in which the blockade effect was recently reported [2]. To this end, we monitor the population dynamics of the multiple-excitation states to identify regimes in which their presence is favored over the single-excitation states. In particular the inequality $P_2/P_1^2 > 1$, where $P_{1(2)}$ is the population of the single(two)-excitation states [41], can be used to signal the antiblockade effect.

2.4 Model description of interacting atoms

To study the blockade and antiblockade effects in the context of ground state neutral atoms, we considered a linear chain of N two-level atoms equally spaced out by a distance of d and distributed along $\hat{x}$ [42, 2]. The atoms interact via induced electric dipole-dipole interaction, through the exchange and emission of virtual and real photons, respectively, [43] and the system is pumped by a laser propagating along $\vec{k} = k\hat{y}$ (k is the pump wave number) with polarization orthogonal to the chain, along $\hat{z}$, with Rabi frequency Ω detuned by Δ from ω_0, where ω_0 is the bare single atom transition frequency.

The dynamics is described by a quantum master equation of the form (with $\hbar = 1$) [2, 42]:

$$\frac{d}{dt}\hat{\rho} = -i\left[\hat{H}, \hat{\rho}\right] + \mathcal{L}(\hat{\rho}), \tag{2.12}$$

where the Hamiltonian is given by:

$$\hat{H} = -\Delta \sum_i \hat{\sigma}_i^+ \hat{\sigma}_i^- - \frac{1}{2}\sum_i \left(\Omega e^{i\vec{k}\cdot\vec{r}_i}\hat{\sigma}_i^+ + \text{H.c.}\right) + \sum_{i,j} \Delta^{ij}\hat{\sigma}_i^+\hat{\sigma}_j^-. \tag{2.13}$$

The $\mathcal{L}(\hat{\rho})$ is a superoperator called *Lindbladian*, which accounts for dissipation effects due to the interaction of the system with the environment (also called a *reservoir*) [44]. $\mathcal{L}(\hat{\rho})$ for this model is given by:

$$\mathcal{L}\left(\hat{\rho}\right) = \frac{1}{2}\sum_{i,j}\Gamma^{ij}\left(2\hat{\sigma}_i^-\hat{\rho}\hat{\sigma}_j^+ - \{\hat{\sigma}_j^+\hat{\sigma}_i^-, \hat{\rho}\}\right). \tag{2.14}$$

The terms Δ^{ij} and Γ^{ij} in the Eqs. (2.13) and (2.14) are, respectively, the elastic and inelastic components given by:

$$\Delta^{ij} = \hat{\epsilon}_i^* \cdot \text{Re}(\mathbf{G}_{ij}) \cdot \hat{\epsilon}_j, \tag{2.15}$$

$$\Gamma^{ij} = \hat{\epsilon}_i^* \cdot 2\text{Im}(\mathbf{G}_{ij}) \cdot \hat{\epsilon}_j. \tag{2.16}$$

These terms describe the long range light-mediated dipole-dipole coupling, where $\hat{\epsilon}_i^*$ is the polarization of the i-th dipole ($\hat{\epsilon}_i^* = \hat{\epsilon}_j^* = \hat{z}$). $\mathbf{G}_{ij}$ is the Green's tensor in free space at position $\mathbf{r}_j$ for a radiating dipole at position $\mathbf{r}_i$, which reads:

$$\mathbf{G}(\mathbf{r}_{ij}) = \frac{3\Gamma}{4}\left[\frac{e^{ikr_{ij}}}{(kr_{ij})^3}\right]\left[\left(k^2r_{ij}^2 + ikr_{ij} - 1\right)\mathbb{I}_3 - \left(k^2r_{ij}^2 - i3kr_{ij} - 3\right)\left(\frac{\mathbf{r}_{ij}\mathbf{r}_{ij}^T}{r_{ij}^2}\right)\right], \quad (2.17)$$

with $\mathbf{r}_{ij} \equiv \mathbf{r}_i - \mathbf{r}_j$. The Green's tensor is a solution of the classical wave equation for the electric field of an oscillating dipole [45].

Equations (2.12),(2.13), and (2.14) were originally derived in the seminal work of Lehmberg [42], in which a general equation of motion for the radiation process of N identical to two-level atoms coupled to a continuum of quantized electromagnetic modes, and an external driving field. These equations were obtained using the Born-Markov approximation — the derivation of the master equation using this approximation is shown in Appendix B.

We can see in Eqs. (2.15),(2.16), and (2.17) that Δ^{ij} and Γ^{ij} are proportional to $1/r_{ij}^3$, just like the Green's tensor from which they are derived. This spatial dependence is a feature of the vectorial model of light, which we use in this work. Differently, the scalar model of light, which is used when the polarization of the dipoles can be disregarded, has the following equations for the elastic and inelastic terms: $\Delta_{ij} = -\frac{\Gamma}{2}\frac{\cos(kr_{ij})}{kr_{ij}}$ and $\Gamma^{ij} = \Gamma\frac{\sin(kr_{ij})}{kr_{ij}}$, that is: proportional to $1/r_{ij}$ [46]. We choose the vectorial model, because it is more sensitive to the inter-atomic distance r_{ij}, which allows us to achieve the blockade and antiblockade effect with a more realistic distance between the atoms.

The terms Δ^{ij} and Γ^{ij} have another important role in our model. To follow the protocol presented in Fig. 2(b) for a general case with an arbitrary number of atoms N, it is necessary to address a single superradiant (SR) [47, 48] eigenstate of the interacting Hamiltonian, and thus the laser detuning must be: $\Delta = \Delta_{SR}$, where Δ_{SR} comes from the SR state, which can be achieved for some specific values of Δ^{ij} and Γ^{ij}. Defining $M^{ij} = \Gamma^{ij} + i\Delta^{ij}$ as the single-excitation coupling matrix [49, 50], the SR state can be identified through the diagonalization of M^{ij} as the eigenstate whose eigenvalue has the largest real part (Γ_{SR}), and the corresponding imaginary part of this eigenvalue is its energy Δ_{SR}. So, to obtain a significant blockade effect a sufficiently small interatomic distance is necessary.

2.5 The sensor method and dressed atoms

A fundamental phenomenon of the light-matter interaction is the resonance fluorescence, consisting of an event in which a two-level system is driven coherently at the same frequency of its natural transition [51]. In the high-excitation regime, the resonance

fluorescence spectral lines acquire a peculiar triplet shape, which was theoretically described by Benjamin Mollow in 1969 [52] and experimentally observed for the first time by Schuda et al. [53] for a sodium atomic beam (and later reported on different platforms [54, 55, 56]), nowadays commonly known as the "Mollow triplet".

The physical explanation of the Mollow triplet arises from the description of a two-level system being driven by an incident laser [57], which, in turn, gives rise to new eigenstates called "dressed states", previously introduced in Sec. 2.3 and formed by a combination of the bare states $|\downarrow, n\rangle$ and $|\uparrow, n-1\rangle$, with $\downarrow$ and $\uparrow$ labeling the atomic *ground* and *excited states*, respectively, and n the number of photons. A set of these states with the same number of excitation constitutes an excitation manifold where the eigenstates are separated by the Rabi Frequency. It is worth noting that the energy difference between two manifolds is equal to the energy difference associated with the corresponding bare states, and the transition between contiguous manifolds is responsible for the Mollow triplet characteristics.

The properties of dressed states have been intensively studied given their fundamental role in describing the Mollow triplet. Several theoretical and experimental studies have demonstrated the existence of correlations between the photons of the triplet peaks [58, 59, 60, 61]. This correlation analysis has been made more complete by resorting to frequency-resolved photon correlations theories, which allows describing qualitatively all the time-orderings of the emitted photons [62, 63, 64]. However, in general, the calculation of correlations in these theories has a heavy computational cost due to increasing complexity, in particular when expanding to higher-order photon-photon correlations $g^{(n)}(\tau)$ ($n \geq 2$). The extension of the discussion to the case of two-photon emission and detection was largely motivated by the experimental works of Aspect et al. in the 1980s [60, 65, 66], in particular the study of resonance fluorescence in the Mollow triplet. These experiments were theoretically described, at first, by Cohen-Tannoudji et al. [59] through a dressed atoms approach. When the correlations between two photons are studied, it is possible to obtain the complete description of all correlations, for any possible frequency combination, not only for the peaks of the triplet [24, 20]. The two-photon correlation spectrum, which provides the second-order correlations for a pair of photon frequencies, reveals the formation of other lines besides the triplet, which correspond to two-photon transitions from one manifold (of dressed states with n photons) to another positioned at two levels below (with dressed states with $n-2$ photons). Some of these two-photon transitions through virtual states (dressed with $n-1$ photons), following *leapfrog processes* [21, 22]. The auxiliary photon in any of these processes is virtual, which results in strong correlations between the emitted pairs [23]. The detailed frequency-resolved correlation spectrum was experimentally obtained by Peiris et al. on a quantum dot [67], confirming that the correlations between the Mollow triplet peaks are a particular case of a more general phenomenon. In Fig. 3 (a) the fluorescence spectrum is presented for a two-level atom

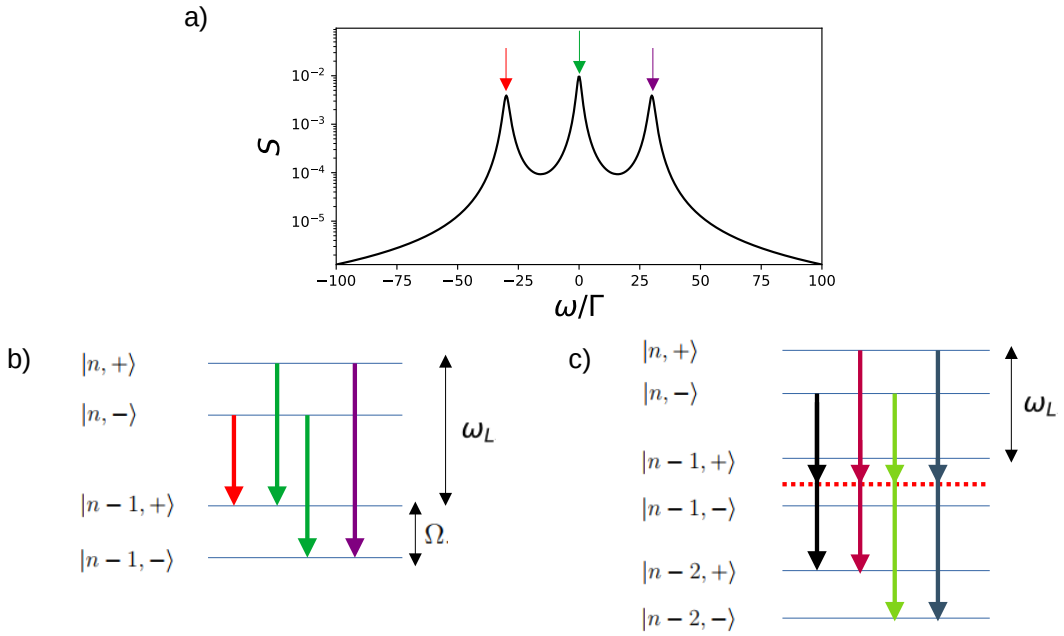

Figure 3 – (a) The fluorescence spectrum for one two-level atom interacting with an incident laser, presenting the Mollow triplet. The triplet peaks are associated with the single-photon emission transitions, shown in the dressed-states picture in (b) with color correspondence. The separation between the dressed states is in terms of the Rabi frequency Ω. In (c) is presented the two-photon emission transitions via a virtual state (red dotted line), which is the so-called leapfrog process. It is pointed out both in (b) and (c) that the transition energy between two neighboring excitation manifolds is ω, i.e.: the incident laser energy has been tuned to induce such transition in the atom. To generate the Mollow triplet in (a), the following parameters were considered: $\Gamma = 1$, $\Omega = 50\Gamma$ and $\Delta = \omega - \omega_0$, where: Γ is the single atom linewidth and Δ is the detuning between the laser energy and the atomic transition energy ω_0. In this case, as aforementioned, we have $\omega = \omega_0$ (laser-atom resonance), so $\Delta = 0$.

interacting with an incident laser, showing the Mollow triplet. The excitation manifold with transitions associated with single-photon emission are depicted in Fig. 3 (b) whose contributions to the triplet peaks are highlighted with corresponding colors. Furthermore, we present in Fig. 3 (c) the representations of some leapfrog processes in the dressed states picture.

With the advances in experimental techniques to control the emission and detection of photons, quantum systems at the single-photon level have been systematically studied, since in this regime there is the strongest manifestation of emission events with a quantum nature. Along with this single-photon resolution came the demand for adjustments and generalizations of the photodetection theory [51]. Indeed, at this level, a more robust theoretical description is needed than that provided by definitions and general mathematical statements, in which the light field is described through abstract properties, from which the

physical meaning may not be easily extracted [68]. In this context, Eberly and Wódkiewics showed how necessary it is to include the physics of the detectors in the description of the light field [69].

A connection between the quantum system and the observer can be done through an input-output formalism, in which the photons inside the system are weakly coupled to a continuum of external modes. Here the external modes are described by the $\hat{A}_\omega$ operator (relative to the frequency ω). In the Heisenberg picture, the output field allows us to compute the time-dependent power spectrum of emission since the density of output photons with frequency ω_1 at time T_1 is given by [19]:

$$S^{(1)}_{\Gamma_1}(\omega_1, T_1) = \langle \hat{A}^\dagger_{\omega_1}(T_1)\hat{A}_{\omega_1}(T_1)\rangle \,. \tag{2.18}$$

The photons multiplicity demands a time and normal ordering (represented by the symbol ":") of the operators [70, 71]. Hence we have:

$$S^{(2)}_{\Gamma_1,\Gamma_2}(\omega_1, T_1, \omega_2, T_2) = \langle : \hat{A}^\dagger_{\omega_1}(T_1)\hat{A}_{\omega_1}(T_1)\hat{A}^\dagger_{\omega_2}(T_2)\hat{A}_{\omega_2}(T_2) : \rangle \,, \tag{2.19}$$

for a two-photon detection: the first (second) photon with frequency $\omega_1(\omega_2)$, at the time $T_1(T_2)$ and captured by the dectector with linewidth $\Gamma_1(\Gamma_2)$. The normalization of $S^{(2)}_{\Gamma_1,\Gamma_2}(\omega_1, T_1; \omega_2, T_2)$ results in a positive and finite second-order correlation function:

$$g^{(2)}_{\Gamma_1,\Gamma_2}(\omega_1, T_1; \omega_2, T_2) = \frac{S^{(2)}_{\Gamma_1,\Gamma_2}(\omega_1, T_1; \omega_2, T_2)}{S^{(1)}_{\Gamma_1}(\omega_1, T_1)S^{(1)}_{\Gamma_2}(\omega_2, T_2)}. \tag{2.20}$$

In general, the calculation of these correlation functions $g^{(M)}_{\Gamma_1,\ldots,\Gamma_M}$ is challenging and involves extensive integrals, making their analytical solution practically intractable for the case $M > 2$. The case $M = 2$ already requires several approximations and algebraic simplifications, limiting the physical treatment of the problem [64, 72]. However, del Valle et al. [19] recently developed a theory of photon correlations, which consists in introducing M sensors to the open quantum system dynamics, where each sensor is a two-level system with annihilation operator $\hat{\xi}_i$ and transition frequency ω_i, which corresponds to the frequency of the photons to be measured by the sensor. To prevent interference in the dynamics of the system itself, the coupling between the sensors and the system, represented by a constant $\epsilon_i = \epsilon$, must be very small.

Under these conditions, the system dynamics in presence of the sensors can be solved. Note that instead of solving the Heisenberg equations and expressing the correlations in terms of the system operators, the intensity correlations function $g^{(2)}_\Gamma(\omega_1, \omega_2)$ is written in terms of the sensor operators:

$$g^{(2)}_\Gamma(\omega_1, \omega_2, \tau) = \lim_{t\to\infty} \frac{\langle \hat{\xi}^\dagger_1(\omega_1, t)\hat{\xi}^\dagger_2(\omega_2, t+\tau)\hat{\xi}_2(\omega_2, t+\tau)\hat{\xi}_1(\omega_1, t)\rangle}{\langle \hat{\xi}^\dagger_1(\omega_1, t)\hat{\xi}_1(\omega_1, t)\rangle \langle \hat{\xi}^\dagger_2(\omega_2, t+\tau)\hat{\xi}_2(\omega_2, t+\tau)\rangle}, \tag{2.21}$$

which makes the computation much simpler [21, 23]. Here, τ is the time interval between detections of the photon with frequency ω_1, which happens at time t, and the photon with frequency ω_2, which happens at $t+\tau$. The sensors are included in the dynamics through the addition of a Hamiltonian term $\hat{H}_s = \sum_s \omega_s \hat{\xi}_s^\dagger \hat{\xi}_s + \epsilon \sum_s \left(E^- \hat{\xi}_s + E^+ \xi_s^\dagger\right)$ and a Lindbladian term $\mathcal{L}_s[\hat{\rho}] = \frac{\Gamma_s}{2} \sum_s \left(2\hat{\xi}_s \hat{\rho} \hat{\xi}_s^\dagger - \hat{\xi}_s^\dagger \hat{\xi}_s \hat{\rho} - \hat{\rho} \hat{\xi}_s^\dagger \hat{\xi}_s\right)$, where Γ_s is the sensor linewidth.

2.6 Cauchy-Schwarz and Bell inequalities

Classical descriptions of the radiation field [73] and local hidden variable theories [74] lead to a series of inequalities that, when violated, indicate non-classicality [75]. Among such inequalities, the Cauchy-Schwarz inequality (CSI) and Bell inequalities (BIs) stand out, since both have already been extensively explored.

The CSI is one of the most important relations in mathematics and can be expressed by:

$$| \langle XY \rangle | \leq \sqrt{\langle X^2 \rangle \langle Y^2 \rangle}, \tag{2.22}$$

where X and Y are random variables. Equation (2.22) indicates that the fluctuation of the product between two random variables is bounded by the products of the autocorrelations of these variables. However, if X and Y are quantum observables, such inequality can be violated, i.e.: quantum correlations between two separate objects can be large enough to overcome their fluctuations, an effect that does not exist in classical physics. BIs refer to a more general problem: the non-local character of quantum mechanics, and the violation of BIs confirms the consistency of quantum mechanics over local hidden variable theories. The first experimental demonstrations of the CSI and BIs violations were obtained in the 1970s for the CSI [76] and in the 1980s for the BIs [65, 66]. Most experiments on the violation of these inequalities involve investigating correlations between photons with different frequencies emitted in multiple-photon processes, such as atomic cascades [65] and four-wave mixing [77, 78].

In quantum optics, the CSI and BIs can be expressed through correlations between electromagnetic field modes operators $\hat{\xi}_i$ and $\hat{\xi}_j$ for $i, j \in (1, 2)$ as in Eq. (2.21). The CSI requires that $[g_{12}^{(2)}]^2 \leq g_{11}^{(2)} g_{22}^{(2)}$ and such relation can be expressed in a more convenient way by the following ratio:

$$R = \frac{[g_{12}^{(2)}]^2}{g_{11}^{(2)} g_{22}^{(2)}}, \tag{2.23}$$

where $R \leq 1$ for a classical field.

The computation of BIs is not as straightforward as that of the CSI and, for most of the works, they are calculated considering polarizing filters. However, we want here to calculate BI based on frequency filtering (sensor method) as established by Muñoz et al.

in [23] (see Sec. 2.5). The resulting frequency-dependent expression reads:

$$B = \sqrt{2}\left|\frac{\langle \hat{a}_1^{\dagger 2}\hat{a}_1^2\rangle + \langle \hat{a}_2^{\dagger 2}\hat{a}_2^2\rangle - 4\langle \hat{a}_1^\dagger \hat{a}_2^\dagger \hat{a}_2 \hat{a}_1\rangle - \langle \hat{a}_1^{\dagger 2}\hat{a}_2^2\rangle - \langle \hat{a}_2^{\dagger 2}\hat{a}_1^2\rangle}{\langle \hat{a}_1^{\dagger 2}\hat{a}_1^2\rangle + \langle \hat{a}_2^{\dagger 2}\hat{a}_2^2\rangle + 2\langle \hat{a}_1^\dagger \hat{a}_2^\dagger \hat{a}_2 \hat{a}_1\rangle}\right|, \tag{2.24}$$

where the BI is violated if $B > 2$ ($\hat{a}_i$ is an arbitrary annihilation operator). This equation can be adapted to the sensor method [21] as follows:

$$B_s = \sqrt{2}\left|\frac{B_{1111} + B_{2222} - 4B_{1221} - B_{1122} - B_{2211}}{B_{1111} + B_{2222} + B_{1221}}\right|, \tag{2.25}$$

where $B_{jklm} = \langle \hat{\xi}_1^\dagger(\omega_j)\hat{\xi}_2^\dagger(\omega_k)\hat{\xi}_2(\omega_1)\hat{\xi}_1(\omega_m)\rangle$.

3 Results

In this section, we will present the results obtained for near-ground state, two-level atomic systems with induced dipole-dipole interactions using the vectorial model (see Sec. 2.4). We performed numerical simulations using the QuTip toolbox [79, 80] (see Appendix C for detailed codes), in which we considered two systems in the steady state with $N = 2$ and $N = 3$ atoms, linearly distributed and with an interparticle spacing of $d = 0.2k^{-1}$.

3.1 The blockade and antiblockade regions

As discussed in Secs. 2.2 and 2.3, we can use $g^{(2)}(0) < 1$ as an indication of the blockade effect, and $P_2/P_1^2 > 1$ of the antiblockade. Indeed, the ratio P_2/P_1^2 is expected to be between one and two for a separable state with $N = 2$ atoms. In Fig. 4, we present the degree of second-order coherence $g^{(2)}(0)$ and the population of the excited states as a function of the Rabi frequency Ω and the detuning Δ for two neutral atoms. We show in Fig. 4(a) the plot of the ratio P_2/P_1^2 as a function of Δ and for a fixed value of Ω ($\Omega/\Gamma = 30$). The ration is larger than one for Δ/Γ in the intervals $[-27.59, -0.58]$ and $[0.58, 88.65]$, indicating the antiblockade effect for this regions. In Fig. 4(b) we present the plot of $g^{(2)}(0)$ as a function of Δ and verify that $g^{(2)}(0) \ll 1$ around $\Delta/\Gamma = -100$, indicating a blockade region. In Fig. 4(c) we show the single- and two-excitation states population, noting that P_1 is always larger than P_2. Indeed, the presence of spontaneous emission makes it harder to populate the double-excited state than the single-excited one. In Fig. 4(d) we show a map of P_2/P_1^2 as a function of Δ and Ω. Here the blockade and antiblockade regions for $\Omega/\Gamma = 30$ are the same as the ones indicated in Fig. 4(a), which is a cut of this map for this value of Ω/Γ. In particular, the ratio P_2/P_1^2 is larger than one for $0 \lesssim \Omega/\Gamma \lesssim 50$ and Δ/Γ in the aforementioned intervals, which is a signature of the antiblockade effect in this region. For larger values of Ω, the pump strength overcomes any interaction-related effects, saturating the atomic system. The atoms then behave almost independently and (anti)blockade is lost.

In Fig. 5, we monitor the same quantities for a chain of three atoms. In Fig. 5(a) we have the plot of P_2/P_1^2 as a function of Δ, where $P_2/P_1^2 > 1$ around $\Delta = 0$, indicating an antiblockade region. In Fig. 5(b) we show $g^{(2)}(0)$ as a function of Δ, where $g^{(2)}(0) \ll 1$ around $\Delta/\Gamma = \pm 150$, indicating a blockade region. In Fig. 5(c) we present the single-, two- and three-excitation states population (respectively: P_1, P_2 and P_3) in which: $P_1 > P_2 > P_3$ for all values of Δ with P_2 very close to P_3. Finally, in Fig. 5(d) we show the map of P_2/P_1^2 as a function of Δ and Ω and the blockade region appears for $\Delta/\Gamma \sim \pm 150$ [as

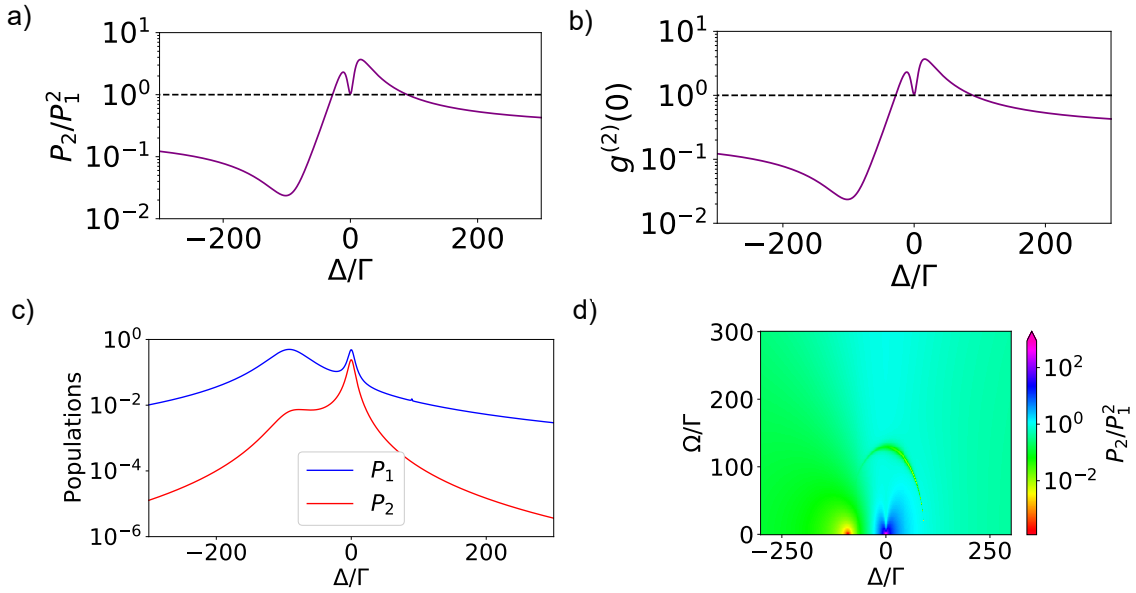

Figure 4 – **(a)** Ratio P_2/P_1^2 as a function of Δ and for a fixed value of Ω ($\Omega = 30\Gamma$), **(b)** intensity-intensity correlation function $g^{(2)}(0)$ as a function of Δ, **(c)** population of the single (blue) and two (red) excitation states population, **(d)** map of the ratio P_2/P_1^2 as a function of Ω and Δ. Here we treated a two-atom system ($N = 2$) spaced by $d = 0.2k^{-1}$ along $\hat{x}$ and incident laser of wave vector $\vec{k} = k\hat{y}$, polarized along $\hat{z}$. The map is on a logarithmic scale

already identified in Fig. 5(b)], P_2/P_1^2 is larger than one for $\Delta/\Gamma = \pm 80$ and $\Delta/\Gamma = 0$, where the antiblockade effect is achieved. We did the simulations here for $N = 3$ with the aim of showing that the appearance of the blockade and antiblockade regions is not a particularity of the $N = 2$ system. In the results which will be presented in the next sections, we focus on simulations for a two-atom system.

From the results presented in this section, we were able to observe that the blockade and antiblockade effects are present in our atomic system. Then, we can obtain more information about the emitted light in these regimes, starting with the energy distribution that will be presented in the next section through the fluorescence spectrum. This will help us find the energy values for the transition that occurs between dressed states associated with a single-photon emission. We will use the sensor method for it, where the spectrum is calculated using the sensor operators, as follows: $S(\omega) = \langle \hat{\xi}_1^\dagger(\omega)\hat{\xi}_1(\omega) + \hat{\xi}_2^\dagger(\omega)\hat{\xi}_2(\omega)\rangle$.

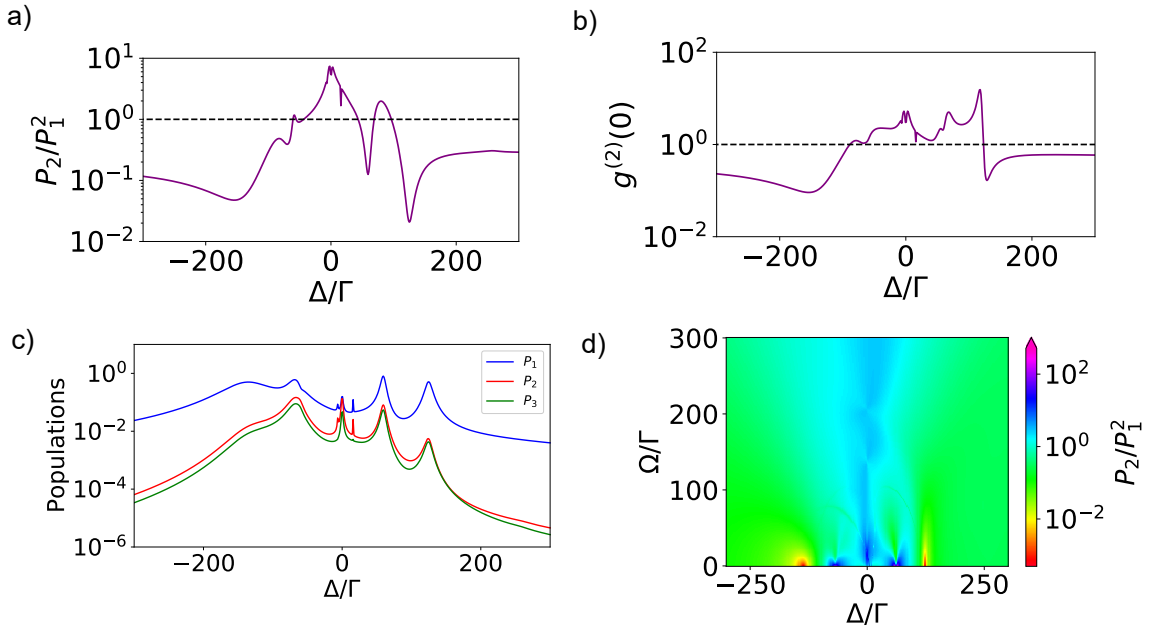

Figure 5 – **(a)** Ratio P_2/P_1^2 as a function of Δ and for a fixed value of Ω ($\Omega = 30\Gamma$), **(b)** intensity-intensity correlation function $g^{(2)}(0)$ as a function of Δ, **(c)** population of the single (blue), two (red) and three (green) excitation states population, **(d)** map of the ratio P_2/P_1^2 as a function of Ω and Δ. Here we treated a three-atoms system ($N = 3$) spaced by $d = 0.2k^{-1}$ along $\hat{x}$ and incident laser of wave vector $\vec{k} = k\hat{y}$, polarized along $\hat{z}$.

3.2 The fluorescence spectrum

Following the approach of Compagno et al. [81] for a single atom dressed by a laser field, the eigenstates of the Hamiltonian at resonance have the following expression:

$$|\pm\rangle = \frac{1}{\sqrt{2}}\left(|\uparrow, n-1\rangle \pm |\downarrow, n\rangle\right), \tag{3.1}$$

where $|\uparrow, n-1\rangle = |\uparrow\rangle \otimes |n-1\rangle$ and $|\downarrow, n\rangle = |\downarrow\rangle \otimes |n\rangle$, with $|\uparrow\rangle$, $|\downarrow\rangle \in \mathcal{H}_a \subset \mathcal{H}$ and $|n\rangle$, $|n-1\rangle \in \mathcal{H}_l \subset \mathcal{H}$, $\mathcal{H}$ is the Hilbert space and $\mathcal{H}_a(\mathcal{H}_l)$ is an subspace of $\mathcal{H}$ associated with the atomic system (laser field). This pair of eigenstates defines an n-excitation manifold where they are split by the Rabi frequency of the incident laser [21]. Thus, for two interacting atoms close together ($kd \ll 1$), the dipole-dipole interactions in Eqs. (2.13) and (2.14) produce two single-excitation eigenstates called symmetric ($|S\rangle$) and anti-symmetric ($|A\rangle$), defined respectively as:

$$|S\rangle = \frac{1}{\sqrt{2}}\left(|\uparrow\downarrow\rangle + |\downarrow\uparrow\rangle\right), \tag{3.2}$$

$$|A\rangle = \frac{1}{\sqrt{2}}\left(|\uparrow\downarrow\rangle - |\downarrow\uparrow\rangle\right). \tag{3.3}$$

As it was done in [81], we will consider the following basis:

$$|\phi_n^1\rangle = |\uparrow\uparrow, n-2\rangle\,, \tag{3.4}$$

$$|\phi_n^2\rangle = |S, n-1\rangle\,, \tag{3.5}$$

$$|\phi_n^3\rangle = |A, n-1\rangle\,, \tag{3.6}$$

$$|\phi_n^4\rangle = |\downarrow\downarrow, n\rangle\,, \tag{3.7}$$

which consists of a four-dimensional subspace of the eigenvectors. We can see that the atomic system and the incident laser field are integrated on this basis, forming the atom-light system, where the number of photons and excitation are conserved, for example: in $|\phi_n^1\rangle$ we have two-excitation ($|\uparrow\uparrow\rangle$) in the atoms and two photons less in the light field ($|n-2\rangle$). The same holds for the other states.

3.2.1 The diagonalization of the Hamiltonian for the two-atom case

The eigenstates can be obtained analytically for the two-atom case since they can be calculated from the diagonalization of the Hamiltonian expressed in equation (2.13). For two atoms, the Hamiltonian is written as follows:

$$\hat{H} = -\Delta(\hat{\sigma}_1^+\hat{\sigma}_1^- + \hat{\sigma}_2^+\hat{\sigma}_2^-) - \frac{\Omega}{2}(\hat{\sigma}_1^+ + \hat{\sigma}_1^- + \hat{\sigma}_2^+ + \hat{\sigma}_2^-). \tag{3.8}$$

The first step is to represent the Hamiltonian matrix in the basis defined in Eqs. (3.4)-(3.7), where the element positioned in the i-th row and in the j-th column (H_{ij}) is given by:

$$H_{ij} = \langle\phi_n^i|\hat{H}|\phi_n^j\rangle\,. \tag{3.9}$$

We thus obtain:

$$\hat{H} = \begin{pmatrix} -2\Delta & -\frac{\Omega}{\sqrt{2}} & 0 & 0 \\ -\frac{\Omega}{\sqrt{2}} & -\Delta+\zeta & 0 & -\frac{\Omega}{\sqrt{2}} \\ 0 & 0 & -\Delta-\zeta & 0 \\ 0 & -\frac{\Omega}{\sqrt{2}} & 0 & 0 \end{pmatrix} \tag{3.10}$$

where $\zeta = \Delta^{12} = \Delta^{21}$. Through the diagonalization of the Hamiltonian expressed in Eq. (3.10), we obtain the following eigenstates:

$$|v_n^1\rangle = |A, n-1\rangle\,, \tag{3.11}$$

$$|v_n^2\rangle = k_1^{(2)}\,|\uparrow\uparrow, n-2\rangle + k_2^{(2)}\,|S, n-1\rangle + k_3^{(2)}\,|\downarrow\downarrow, n\rangle\,, \tag{3.12}$$

$$|v_n^3\rangle = k_1^{(3)}\,|\uparrow\uparrow, n-2\rangle + k_2^{(3)}\,|S, n-1\rangle + k_3^{(3)}\,|\downarrow\downarrow, n\rangle\,, \tag{3.13}$$

$$|v_n^4\rangle = k_1^{(4)}\,|\uparrow\uparrow, n-2\rangle + k_2^{(4)}\,|S, n-1\rangle + k_3^{(4)}\,|\downarrow\downarrow, n\rangle\,. \tag{3.14}$$

These eigenvectors are the n-excitation manifold for our system and $k_l^{(m)}$ are given by:

$$k_1^{(2)} = -1 - \frac{1}{2\Omega^2}\left[2\zeta - 2\Delta - \lambda_1(\zeta,\Delta,\Omega)\right]\lambda_1(\zeta,\Delta,\Omega),$$

$$k_2^{(2)} = \frac{-\lambda_1(\zeta,\Delta,\Omega)}{\sqrt{2}\Omega},$$

$$k_1^{(3)} = -1 - \frac{1}{2\Omega^2}\left[2\zeta - 2\Delta - \lambda_2(\zeta,\Delta,\Omega)\right]\lambda_2(\zeta,\Delta,\Omega),$$

$$k_2^{(3)} = \frac{-\lambda_2(\zeta,\Delta,\Omega)}{\sqrt{2}\Omega},$$

$$k_1^{(4)} = -1 - \frac{1}{2\Omega^2}\left[2\zeta - 2\Delta - \lambda_3(\zeta,\Delta,\Omega)\right]\lambda_3(\zeta,\Delta,\Omega),$$

$$k_2^{(4)} = \frac{-\lambda_3(\zeta,\Delta,\Omega)}{\sqrt{2}\Omega},$$

with

$$k_3^{(2)} = k_3^{(3)} = k_3^{(4)} = 1.$$

The functions $\lambda_1(\zeta,\Delta,\Omega)$, $\lambda_2(\zeta,\Delta,\Omega)$, and $\lambda_3(\zeta,\Delta,\Omega)$ can be written as follows:

$$\lambda_1(\zeta,\Delta,\Omega) = \frac{2}{3}(\zeta - 3\Delta) + 2\frac{F(\zeta,\Delta,\Omega)}{G(\zeta,\Delta,\Omega)} + \frac{1}{3\sqrt[3]{2}}M(\zeta,\Delta,\Omega),$$

$$\lambda_2(\zeta,\Delta,\Omega) = \frac{2}{3}(\zeta - 3\Delta) - (1+i\sqrt{3})\frac{F(\zeta,\Delta,\Omega)}{G(\zeta,\Delta,\Omega)} - \frac{1}{6\sqrt[3]{2}}(1-i\sqrt{3})M(\zeta,\Delta,\Omega),$$

$$\lambda_3(\zeta,\Delta,\Omega) = \frac{2}{3}(\zeta - 3\Delta) - (1-i\sqrt{3})\frac{F(\zeta,\Delta,\Omega)}{G(\zeta,\Delta,\Omega)} - \frac{1}{6\sqrt[3]{2}}(1+i\sqrt{3})M(\zeta,\Delta,\Omega),$$

where $F(\zeta,\Delta,\Omega)$, $G(\zeta,\Delta,\Omega)$, and $M(\zeta,\Delta,\Omega)$ are defined as:

$$F(\zeta,\Delta,\Omega) = \zeta^2 + 3(\Delta^2 + \Omega^2),$$

$$G(\zeta,\Delta,\Omega) = 3\Big[\zeta^3 + \frac{9}{2}\zeta(\Omega^2 - 2\Delta^2) + \frac{3\sqrt{3}}{2}\sqrt{-4\zeta^4\Delta^2 - 4(\Omega^2+\Delta^2)^3 - \zeta^2(\Omega^4 + 20\Delta^2\Omega^2 - 8\Delta^4)}\Big]^{1/3},$$

$$M(\zeta,\Delta,\Omega) = \Big[16\zeta^3 - 144\zeta\Delta^2 + 72\zeta\Omega^2 + 8\sqrt{[2\zeta^3 + 9\zeta(\Omega^2 - 2\Delta^2)]^2 - 4[\zeta^2 + 3(\Omega^2+\Delta^2)]^3}\Big]^{1/3}.$$

The dressed states are characterized by the superposition of different atomic and field states, as shown in Eqs. (3.11)-(3.14). The eigenstate $|v_n^1\rangle$, which contains the anti-symmetric atomic state $|A\rangle$, however, does not couple to any other atom-field state and does not participate substantially in the intensity of the fluorescence spectrum. A consequence, the n-excitation manifold reduces to the triplet, which here is given by $|v_n^2\rangle$, $|v_n^3\rangle$, and $|v_n^4\rangle$, with the following energy differences:

$$\delta_{ij} = -\delta_{ji} = E_n^i - E_n^j. \tag{3.15}$$

In the light of the dressed state picture analytically derived in this subsection, we will now discuss the results of our simulations for $N = 2$ atoms spaced by $d = 0.2k^{-1}$ and pumped by a laser with Rabi frequency $\Omega/\Gamma = 30$.

3.2.2 The fluorescence spectrum for the resonant case

In Fig. 6(a) we have the dressed-state structure for two interacting atoms with $\Delta/\Gamma = 0$ (resonance), which presents the following eigenstates:

$$|v_n^1\rangle = 0.20\,|\uparrow\uparrow, n-2\rangle + 0.96\,|S, n-1\rangle + 0.20\,|\downarrow\downarrow, n\rangle\,, \tag{3.16}$$

$$|v_n^2\rangle = |A, n-1\rangle\,, \tag{3.17}$$

$$|v_n^3\rangle = 0.68\,|\uparrow\uparrow, n-2\rangle - 0.28\,|S, n-1\rangle + 0.68\,|\downarrow\downarrow, n\rangle\,, \tag{3.18}$$

$$|v_n^4\rangle = -0.71\,|\uparrow\uparrow, n-2\rangle + 0.71\,|\downarrow\downarrow, n\rangle\,. \tag{3.19}$$

In Fig. 6(b) we compare the fluorescence spectra for both interacting (black curve) and non-interacting two-atom system ($d = 100k^{-1}$) (green curve). We can see that in the case of non-interacting atoms, the spectrum of the single atom (Mollow triplet [52, 53]) is reproduced. In the case of interacting atoms we also have a central peak, which originates

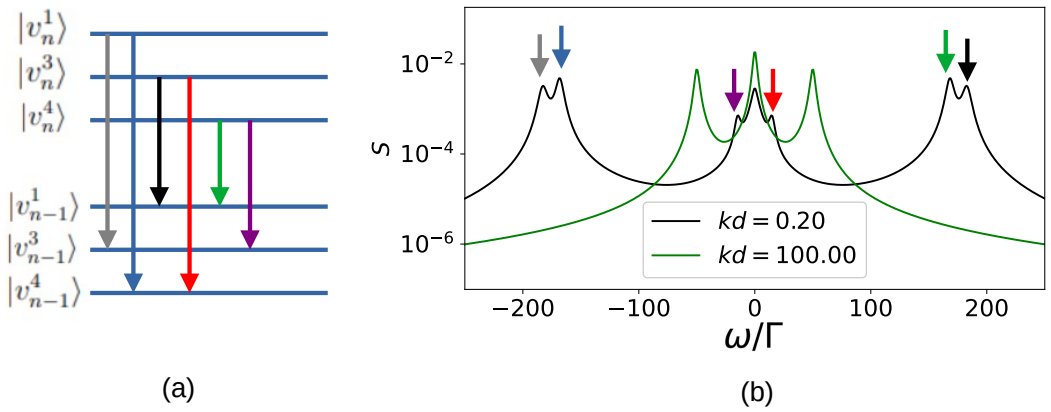

Figure 6 – (a) The dressed state structure for two interacting atoms with $\Delta/\Gamma = 0$ (resonance) (b) The fluorescence spectrum for non-interacting atoms (green) with $d = 100k^{-1}$ and two interacting atoms (black) with $d = 0.2k^{-1}$ and the same other parameters as in (a). The arrows in (b) refer to the transitions presented in (a) (same color code).

from the transition $|v_n^i\rangle \to |v_{n-1}^i\rangle$. In other words, this central peak in the fluorescence spectrum means that the atomic state is not changed, characterizing a one-photon emission resonant with the incident laser. The transformation of the side peaks into triplets for strongly interacting atoms corresponds to resonant frequencies $\pm\Delta_{ij}$ related to transitions $|v_n^i\rangle \to |v_{n-1}^{j\neq i}\rangle$ [represented by the arrows in Fig. 6(a) and (b)]. These peaks are absent for the single atom and non-interacting atoms cases.

3.2.3 Fluorescence spectrum in the blockade regime

In Fig. 7(a) we show the dressed-state scheme for a two-atom system in the blockade region ($\Delta = \Delta_{\mathrm{SR}} = -101.56\Gamma$). This value of detuning corresponds to the global minimum in the plot of $g^{(2)}(0)$ presented in Fig. 4(b) and coincides with the value of Δ_{SR} calculated via the diagonalization of the linear-optics matrix M^{ij} (as described in Sec. 2.4). We have the following eigenstates for this case:

$$|v_n^1\rangle = 0.99\,|\uparrow\uparrow, n-2\rangle - 0.11\,|S, n-1\rangle + 0.011\,|\downarrow\downarrow, n\rangle\,, \tag{3.20}$$

$$|v_n^2\rangle = |A, n-1\rangle\,, \tag{3.21}$$

$$|v_n^3\rangle = 0.090\,|\uparrow\uparrow, n-2\rangle + 0.76\,|S, n-1\rangle - 0.64\,|\downarrow\downarrow, n\rangle\,, \tag{3.22}$$

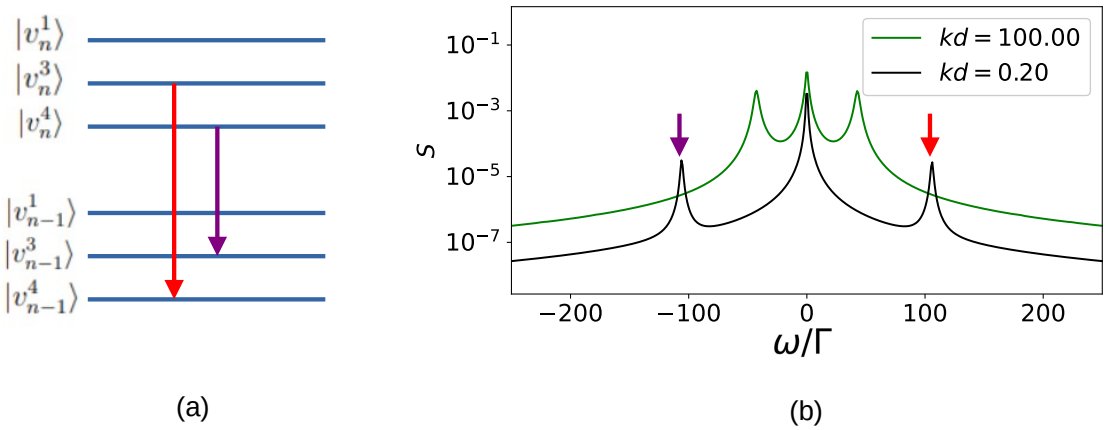

Figure 7 – **(a)** The dressed states structure for two interacting atoms with $\Delta/\Gamma = -101.56$ (blockade regime) **(b)** The fluorescence spectrum for non-interacting atoms (green) with $d = 100k^{-1}$ and two interacting atoms (black) with the same other parameters which was presented in **(a)**. The arrows in (b) refer to the transitions presented in (a) (same color code).

$$|v_n^4\rangle = 0.062\,|\uparrow\uparrow, n-2\rangle + 0.64\,|S, n-1\rangle + 0.76\,|\downarrow\downarrow, n\rangle\,. \tag{3.23}$$

We can see in Fig. 7 that the transitions involving the eigenstate $|v_n^1\rangle$ do not correspond to any peak in the fluorescence spectrum. Indeed, from the expression for $|v_n^1\rangle$ in Eq. (3.20) the two-excitation state coefficient is very close to unity (this quantity is associated with the probability of occupation of the state) and thus $|v_n^1\rangle \approx |\uparrow\uparrow, n-2\rangle$. Therefore, in the blockade regime, where multiple excitations are inhibited, the state of the system has practically no component of $|v_n^1\rangle$, and transitions involving this eigenstate do not appear as a peak in the fluorescence spectrum.

3.2.4 Fluorescence spectrum for the antiblockade regime

In Fig. 8 we present the same dressed-state picture for an interacting two-atom system, but choosing $\Delta/\Gamma = 15.85$. With this detuning, the ratio P_2/P_1^2 reaches its global maximum, as shown in Fig. 4(a), corresponding to an antiblockade regime. In this case, we have the following eigenvectors associated with the system:

$$|v_n^1\rangle = 0.24\,|\uparrow\uparrow, n-2\rangle + 0.96\,|S, n-1\rangle + 0.17\,|\downarrow\downarrow, n\rangle\,, \tag{3.24}$$

$$|v_n^2\rangle = |A, n-1\rangle\,, \tag{3.25}$$

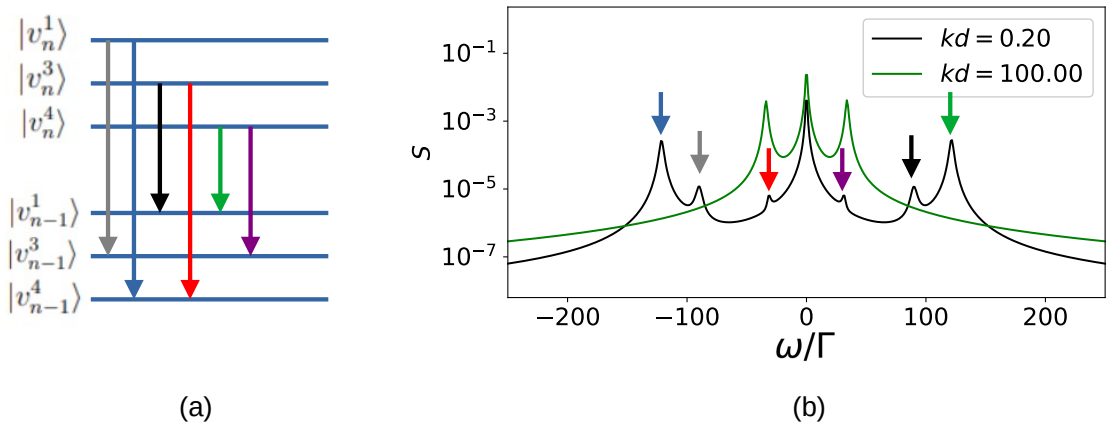

Figure 8 – **(a)** Dressed state structure for two interacting atoms with $\Delta/\Gamma = -15.85$ (antiblockade regime). **(b)** Fluorescence spectrum for non-interacting atoms (green) with $d = 100k^{-1}$ and two interacting atoms (black) with the same other parameters which was presented in **(a)**. The arrows in (b) refer to the transitions presented in (a) (same color code).

$$|v_n^3\rangle = 0.96\,|\uparrow\uparrow, n-2\rangle - 0.21\,|S, n-1\rangle - 0.16\,|\downarrow\downarrow, n\rangle\,, \tag{3.26}$$

$$|v_n^4\rangle = 0.12\,|\uparrow\uparrow, n-2\rangle - 0.21\,|S, n-1\rangle + 0.97\,|\downarrow\downarrow, n\rangle\,. \tag{3.27}$$

3.2.5 Conclusions about the fluorescence spectrum

In the spectra presented in this section, we analyzed the single-photon emission for the blockade and antiblockade regime in the dressed-states picture, compared with the case in resonance. We saw that in the blockade regime the eigenstate $|v_n^1\rangle$, strongly associated with the two-excitation state, has its transitions inhibited — which does not occur in the antiblockade regime. In the next section, we will continue studying the emitted light, but focusing on the correlations between the photons.

3.3 Photon-Photon correlations

The single-photon transitions were shown in the spectra (Figs. 6, 7, and 8). In order to investigate correlations between emitted photons we compute the photon-photon correlations $g_\Gamma^{(2)}(\omega_1, \omega_2)$ introduced in Eq. (2.21). We present in Figs. 10, 11, and 12 maps

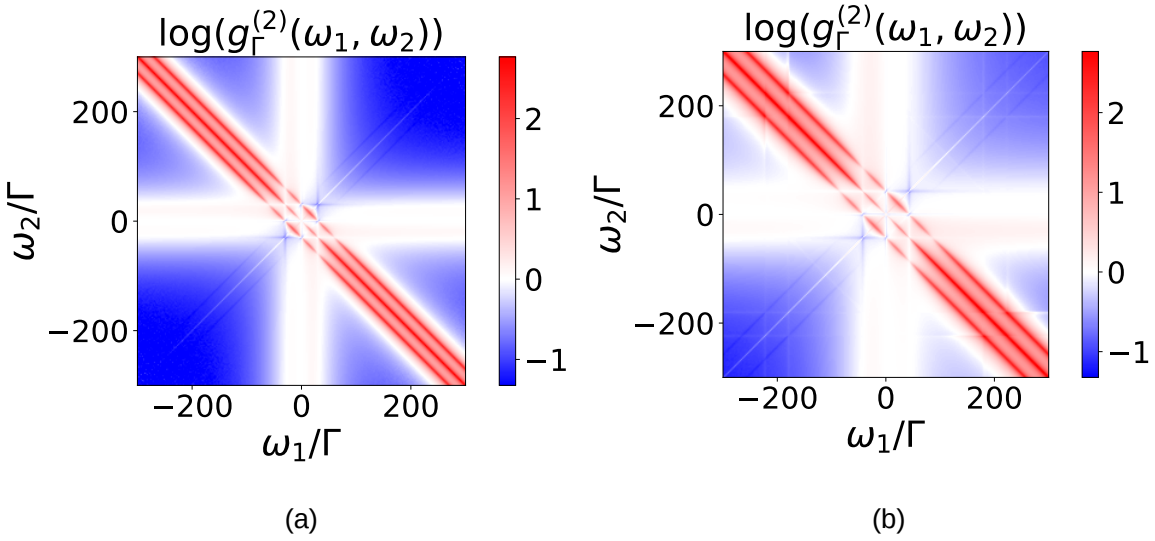

Figure 9 – **(a)** The $g^{(2)}_\Gamma(\omega_1,\omega_2)$ map for a single atom with $\Delta/\Gamma = 0$ (resonance). **(b)** The $g^{(2)}_\Gamma(\omega_1,\omega_2)$ map for a two-atom system with $\Delta/\Gamma = -101.56$ (blockade regime).

for $g^{(2)}_\Gamma(\omega_1,\omega_2)$ in terms of the sensor frequencies ω_s/Γ (for $s = 1, 2$) for three situations: a resonant pumping, the blockade regime, and the antiblockade regime for a two-atom system. From these maps we monitor the two-photon emission correlations associated with opposite sidebands $[g^{(2)}(\delta_{ij}, -\delta_{ij})]$, equal sidebands $[g^{(2)}(\delta_{ij}, \delta_{ij})]$, and cross sidebands $[g^{(2)}(\delta_{ij}, \delta_{i'j'})$, with $i \neq i'$ and $j \neq j']$.

3.3.1 The single atom and the blockade regime: a superatom picture

The blockaded system can be described in a *superatom picture* [2, 34]: the single-excitation, collective state and the many-body ground state play the respective role of the excited and ground state of an effective two-level system. This effective single atom (superatom), however, decays following the collective mode linewidth, here the superradiant decay rate Γ_{SR} instead of the single atom linewidth Γ. Furthermore, the strong interaction promotes the antibunching of the light emitted by the atoms (again, since multiple excitations are inhibited) — we can see in Fig. 9 (a) and (b) that the map associated with the blockade regime is qualitatively close to the single atom map, which corroborates with the superatom picture.

3.3.2 Two atoms and a Resonant Driving

Let us discuss here the case of two atoms resonantly driven by a laser. In the map of Fig. 10, the gray circle symbol represents the transition $|v^1_n\rangle \to |v^3_{n-1}\rangle \to |v^1_{n-2}\rangle$ between

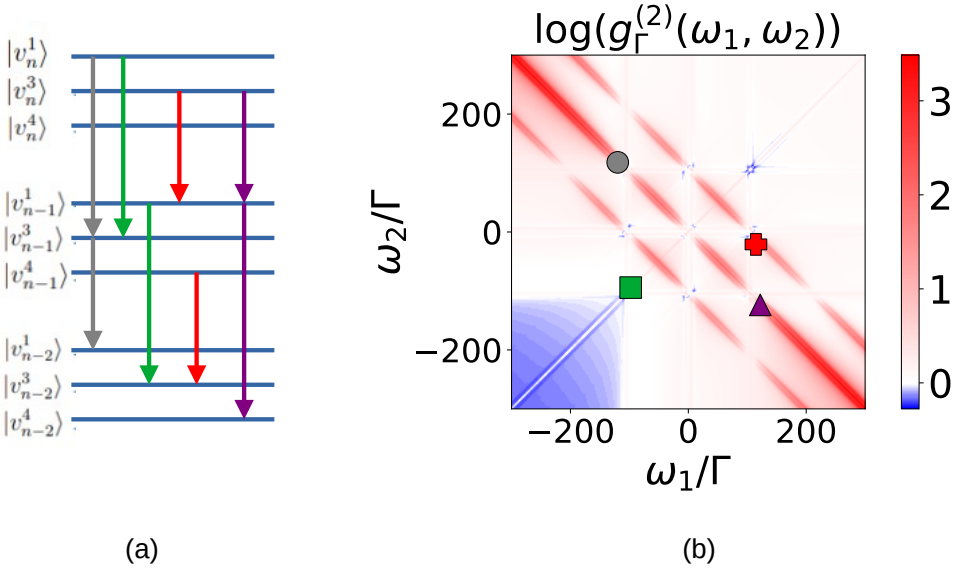

Figure 10 – **(a)** Emission of two photons from opposite sidebands $\omega_1 = -\omega_2$ (gray) equal sidebands $\omega_1 = \omega_2$ (green) and cross sidebands $\omega_1 \neq \omega_2$ (red and purple) in the dressed-states picture for a two-atom system near ground state with $\Delta/\Gamma = 0$ (resonance). **(b)** Map of the photon-photon correlations function $g_\Gamma^{(2)}(\omega_1, \omega_2)$ associated with the dressed-states scheme described in (a).

opposite sidebands $g_\Gamma^{(2)}(\delta_{13}, -\delta_{13})$, an allowed path of relaxation for which $\delta_{13}/\Gamma = -109.77$ and $g_\Gamma^{(2)}(\delta_{13}, -\delta_{13}) > 1$, and it exhibits photon bunching. We verified that the smallest value of the photon-photon correlation function for $\omega_1 = -\omega_2$ (along the main anti-diagonal) is $g_\Gamma^{(2)}(\omega_1, \omega_2) = 1.64$, which implies that the photon bunching holds for all transitions $|v_n^i\rangle \rightarrow |v_{n-1}^j\rangle \rightarrow |v_{n-2}^i\rangle$. The green square symbol represents the two-photon emission from the transitions $|v_n^1\rangle \rightarrow |v_{n-1}^3\rangle$ followed by $|v_{n-1}^1\rangle \rightarrow |v_{n-2}^3\rangle$ (equal sidebands). This is an allowed path of relaxation where we have $g_\Gamma^{(2)}(\delta_{13}, \delta_{13}) > 1$, indicating photon bunching, again. We also verified that the smallest value of $g_\Gamma^{(2)}(\omega_1, \omega_2)$ for $\omega_1 = \omega_2$ is 1.22, which implies that the photon bunching also holds for all transitions with $\omega_1 = \omega_2$ (main diagonal). Note that in the work of Darsheshdar et al. [21] antibunching regions appear for $\omega_1 = \omega_2$ in the case of resonance. However, it is important to observe that in the aforementioned work the scalar model of light was used, which demands smaller interatomic distances for strong bunching and antibunching effects to appear. These two factors change the interaction between the atoms, which is a possible explanation for the appearance of antibunching regions in [21] and not here.

For processes involving a two-photon emission with cross sidebands, $g_\Gamma^{(2)}(\pm\delta_{ij}, \pm\delta_{i',j'})$ with $(i, j) \neq (i', j')$, we have the participation of three distinct atomic states. This requires a more careful analysis since photons with different frequencies are emitted in a specific

order. For example, let us consider two transitions of this type:

$$|v_n^3\rangle \rightarrow |v_{n-1}^1\rangle \text{ followed by } |v_{n-1}^4\rangle \rightarrow |v_{n-2}^3\rangle\,, \tag{3.28}$$

$$|v_n^3\rangle \rightarrow |v_{n-1}^1\rangle \rightarrow |v_{n-2}^4\rangle\,. \tag{3.29}$$

The first case (3.28) is represented by the red cross symbol in the map and is a non-allowed path of relaxation, since $\langle v_{n-1}^1|v_{n-1}^4\rangle = 0$, which indicates that these states are orthogonal. Differently, the second case (3.29), which is represented by the triangle symbol, is an allowed path of relaxation.

3.3.3 Blockade Regime

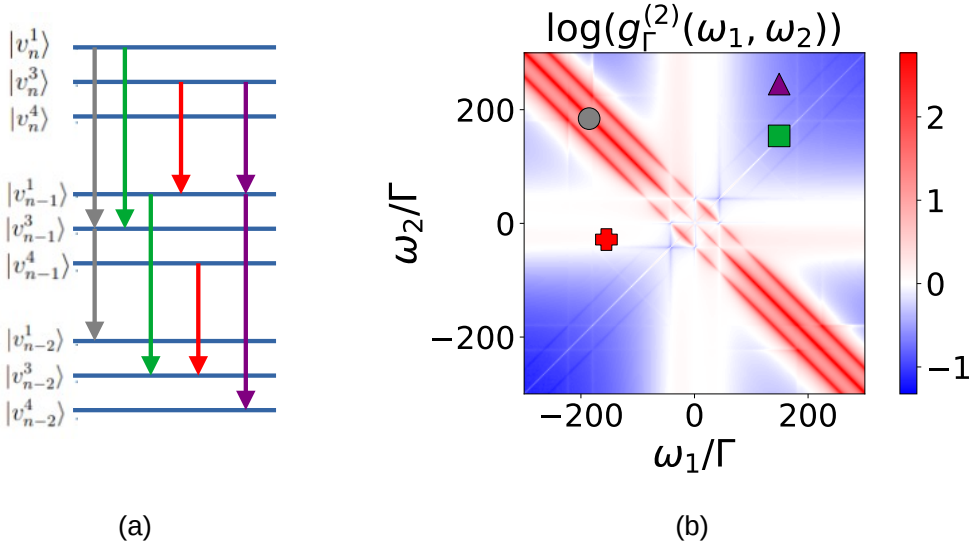

Figure 11 – **(a)** The emission of two photons from opposite sidebands $\omega_1 = -\omega_2$ (gray) equal sidebands $\omega_1 = \omega_2$ (green) and cross sidebands $\omega_1 \neq \omega_2$ (red and purple) in the dressed-states picture for a two-atom system near ground state with $\Delta/\Gamma = -101.56$ (blockade regime). **(b)** The map for the photon-photon correlations function $g_\Gamma^{(2)}(\omega_1, \omega_2)$ associated with the dressed-states scheme described in (a).

In Fig. 11 we present the $g_\Gamma^{(2)}(\omega_1, \omega_2)$ map for the blockade regime ($\Delta/\Gamma = -101.56$). We can see that in this regime characterized by the inhibition of multiple-excitation state, we have more antibunching regions ($g_\Gamma^{(2)}(\omega_1, \omega_2) < 1$). Indeed, comparing with the resonance case, it is possible to observe that two of the transitions highlighted on the map (purple triangle and green square) are in antibunching regions.

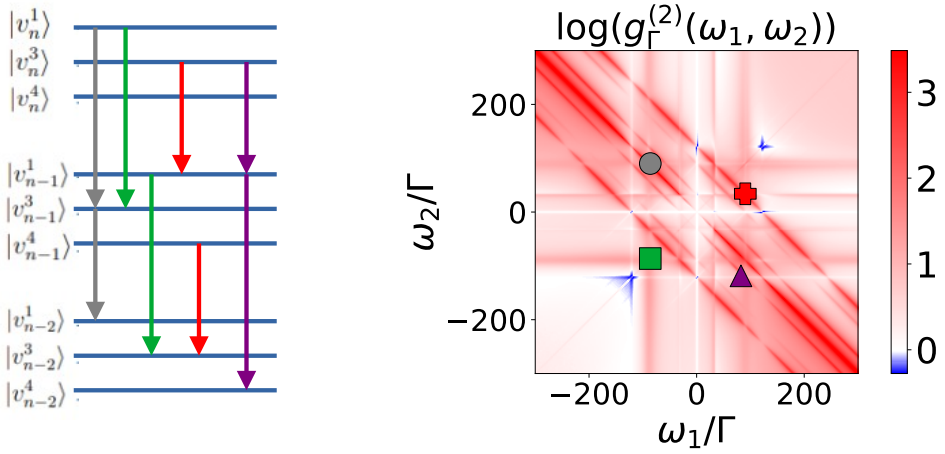

(a) (b)

Figure 12 – **(a)** The emission of two photons from opposite sidebands $\omega_1 = -\omega_2$ (gray) equal sidebands $\omega_1 = \omega_2$ (green) and cross sidebands $\omega_1 \neq \omega_2$ (red and purple) in the dressed-states picture for a two-atom system near ground state with $\Delta/\Gamma = 15.85$ (blockade regime). **(b)** The map for the photon-photon correlations function $g_\Gamma^{(2)}(\omega_1, \omega_2)$ associated with the dressed-states scheme described in (a).

3.3.4 Antiblockade Regime

In Fig. 12 we show the $g^{(2)}(\omega_1, \omega_2)$ map for the antiblockade regime ($\Delta/\Gamma = 15.85$). We can see an increase of bunching regions ($g_\Gamma^{(2)}(\omega_1, \omega_2) > 1$) and in the spacing between the antidiagonal lines as compared with the same maps for the resonance and blockade case (see Figs. 10 and 11). More antidiagonal lines also appear on the map for the antiblockade regimes when compared to the map with the same ranges of ω_1 and ω_2 of the blockade regime. The increase in bunching regions is due to the favored emission of pairs of photons, characteristic of this regime. The differences related to the number and separation of the antidiagonal lines are consequences of the dressed-state structure, resulting from the system interactions in each regime.

3.3.5 Intensity of the emitted light: comparing three regimes

In Fig. 13 we show the second-order correlation function in terms of sensor operators (we use this name because it has the same information of $G^{(2)}$ defined in Eq. (2.10)) $G^{(2)} = \langle \xi_1^\dagger \xi_2^\dagger \xi_2 \xi_1 \rangle$ for: (a) the resonance case, (b) the blockade regime, and (c) the antiblockade regime. We can observe that in the antiblockade regime there are just a few regions of high correlations, which indicates that, although the antiblockade regime facilitates the

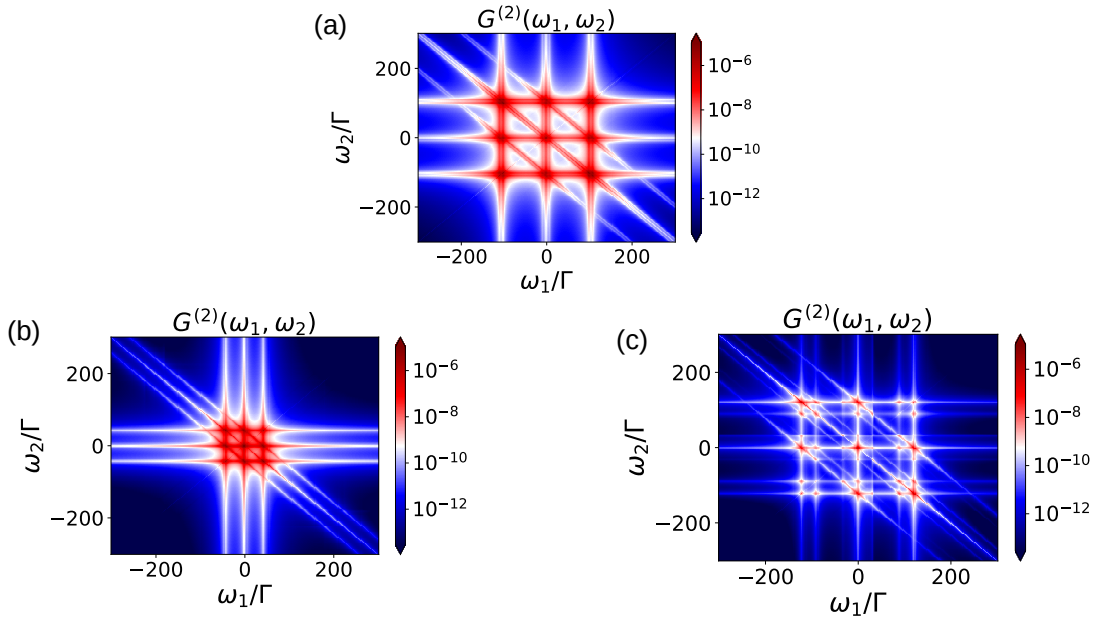

Figure 13 – The map of the photon emission intensity for a two-atom system in **(a)** resonance ($\Delta/\Gamma = 0$), **(b)** blockade regime ($\Delta/\Gamma = -101.56$) and **(c)** antiblockade regime ($\Delta/\Gamma = 15.85$).

emission of two correlated photons, this occurs with low photon flux: these pairs of photons are rare events.

In the next section, we will study the so-called leapfrog processes, discussed in Sec. 2.5. The photons emitted from this type of transitions are strongly correlated, non-classical, and entangled. Thus we can use Cauchy-Schwarz and Bell inequalities to identify such features, since their violation implies non-classicality and entanglement, as discussed in Sec. 2.6

3.4 Leapfrog Processes

The transitions described in the previous section involve two-photon emission processes related to real transitions, i.e. transitions between two manifolds through an intermediate state present in the dressed-state picture. There are other types of two-photon transitions where the intermediate state is not contained in the dressed-state picture. In this case, this state is called a *virtual state* and the two-photon emission associated with it is a *leapfrog process* [24].

The pair of photons emitted during such a leapfrog process is characterized by correlations much stronger than the two-photon emission through real states. Its quantum nature was demonstrated for these single-emitters by violations of the Cauchy-Schwarz (CSI) and Bell (BI) inequalities [82]. In particular, the energy of each photon does not

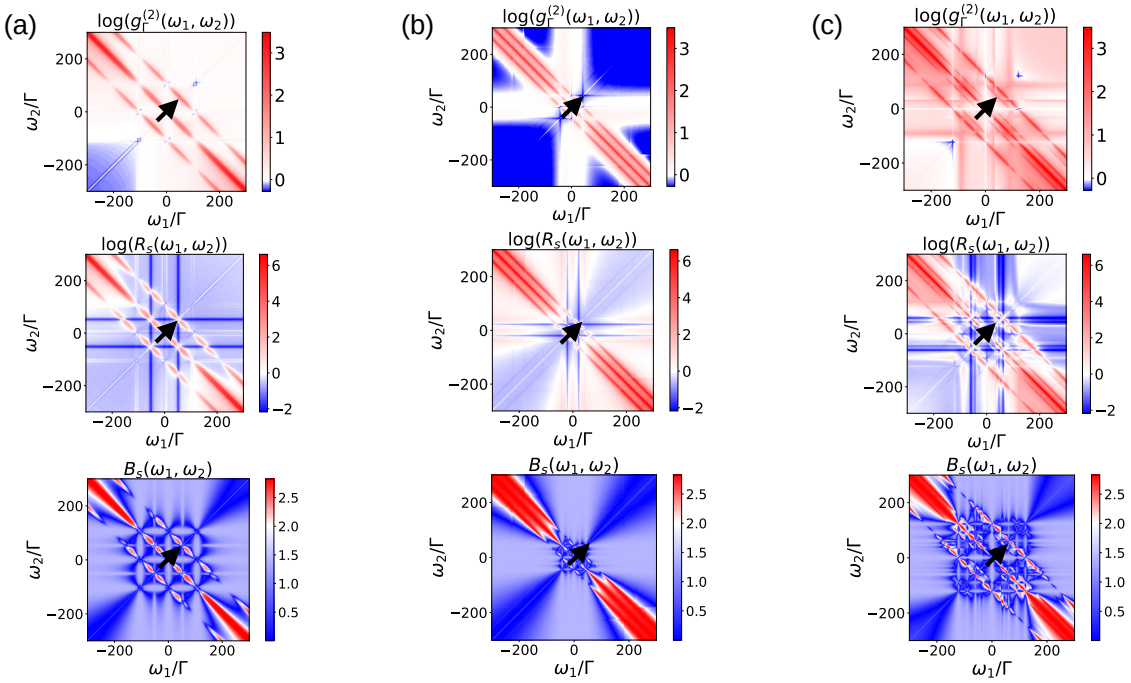

Figure 14 – Maps of $g_\Gamma^{(2)}(\omega_1,\omega_2)$ — same as Figs 10, 11 and 12, but repeated here for the sake of comparison — Cauchy-Schwarz Inequality ($R_s(\omega_1,\omega_2)$) and Bell Inequality ($B_s(\omega_1,\omega_2)$) for (a) the resonance case, (b) the blockade regime and (c) the antiblockade regime.

need to match the energy of a specific single-photon transition, only the sum of these photons' energies needs to match the energy of an existing two-photon transition. In other words, the relations $\omega_1+\omega_2=0$ and $\omega_1+\omega_2=\pm\delta_{ij}$ must be satisfied, which means that the leapfrog process corresponds to anti-diagonal lines in the maps in Figs. 10, 11, and 12. As discussed in Sec. 2.6, the non-classicality of such correlations can be evidenced by the violation of the CSI ($R>1$), where R is given by equation (2.23), and by the violation of the BI expressed by $B>2$, where B is given by equation (2.25).

We can see in all maps of $R_s(\omega_1,\omega_2)$ and $B_s(\omega_1,\omega_2)$ in Fig. 14 that the CSI and BI are violated at most points of the anti-diagonal lines, which correspond to leapfrog processes. Furthermore, we discussed in Sec 2.6 that the violation of the CSI (BI) implies non-classicality (non-locality). Thus if $R_s(\omega_1,\omega_2)>1$ and $B_s(\omega_1,\omega_2)>2$ for a pair of photons with a frequency combination (ω_1,ω_2), the associated two-photon state has a non-classical nature and is entangled. If $g_\Gamma^{(2)}(\omega_1,\omega_2)>1$, the photons are strongly correlated. Thus, the maps indicate frequency regions where the system generates pair of photons strongly correlated, non-classical, and entangled (we pointed out one example with a black arrow in Fig. 14). The identification of non-classical correlations for our atomic system in the resonance, blockade, and antiblockade regimes is the main result of this work, together with the characterization of each regime, as presented in Sec. 3.1.

4 Conclusions

In conclusion, we have conducted a study of the blockade effect, where multiple-excitation states are weakly populated for near-ground state neutral two-level atoms in the subwavelength regime, in which induced dipole-dipole interactions are strong enough to generate this effect [2]. We identified the regime of antiblockade, where multiple-excitation states are preferentially populated, for a two- and three-atom system, using the ratio $P_2/P_1^2 > 1$ as the main indicator of the antiblockade phenomenon [41]. We then studied the generation of pairs of correlated photons for these regimes in a two-atom system and compared it with the case of resonant driving. We characterized the emitted light with different frequencies using the sensor method and presented the fluorescence spectrum of the coupled system, photon-photon correlations, and Cauchy-Schwarz and Bell inequalities.

Based on the fluorescence spectrum, we studied the transitions between excitation manifolds in the dressed-state picture. The fluorescence provides another signature of the blockade effect since the transitions associated with the two-excitation states do not appear in the spectrum, indicating inhibition of such state.

From the photon-photon correlations, we could observe for which combinations of frequencies (ω_1, ω_2) bunching or antibunching occurs. Furthermore, we observed that the antibunching areas in the second-order correlation maps are wider for the blockade regime than for the antiblockade regime. Conversely, the bunching areas are wider for the antiblockade case than for the blockade case, consistent with the nature of these phenomena.

From the Cauchy-Schwarz and Bell inequalities maps, we characterized the non-classical nature of the emitted pairs of photons. These pairs are produced through virtual transitions — the so-called leapfrog processes. We note that similar results on the pairs of the photon, using the sensor method, have been reported for atomic systems using the scalar model of light [21]. Our work with the vectorial model of light, however, allowed us to achieve collective regimes (i.e. blockade and antiblockade effects) making simulations for an atomic ensemble using more realistic interparticle distances than those demanded by the scalar model.

In the context of the model studied and the results obtained in this work, several questions remain open: the scaling of these effects with atom number ($N > 2$), the role of specific geometries (atomic ring, lattices, etc.), and disorder. The many-atom case will certainly hold new surprises since many more complex atom-light manifolds are present.

References

1 PRITCHARD, J. *Cooperative Optical Non-Linearity in a Blockaded Rydberg Ensemble*. [S.l.]: Springer Theses, 2012.

2 CIDRIM, A. et al. Photon blockade with ground-state neutral atoms. *Phys. Rev. Lett.*, American Physical Society, v. 125, p. 073601, Aug 2020. Disponível em: <https://link.aps.org/doi/10.1103/PhysRevLett.125.073601>.

3 GUTZLER, R. et al. Light–matter interaction at atomic scales. *Nature Review Physics*, Nature, -, n. 3, p. 441 – 453, abr. 2021. Disponível em: <https://doi.org/10.1038/s42254-021-00306-5>.

4 OH, J. et al. Sirius: a prototype astronomical intensity interferometer using avalanche photodiodes in linear mode. *Monthly Notices of the Royal Astronomical Society*, v. 500, n. 4, p. 5630–5638, 11 2020. ISSN 0035-8711. Disponível em: <https://doi.org/10.1093/mnras/staa3584>.

5 AMTHOR, T. et al. Evidence of antiblockade in an ultracold rydberg gas. *Phys. Rev. Lett.*, American Physical Society, v. 104, p. 013001, Jan 2010. Disponível em: <https://link.aps.org/doi/10.1103/PhysRevLett.104.013001>.

6 CARR, A. W.; SAFFMAN, M. Preparation of entangled and antiferromagnetic states by dissipative rydberg pumping. *Phys. Rev. Lett.*, American Physical Society, v. 111, p. 033607, Jul 2013. Disponível em: <https://link.aps.org/doi/10.1103/PhysRevLett.111.033607>.

7 SHAO, X.-Q. et al. Stationary three-dimensional entanglement via dissipative rydberg pumping. *Phys. Rev. A*, American Physical Society, v. 89, p. 052313, May 2014. Disponível em: <https://link.aps.org/doi/10.1103/PhysRevA.89.052313>.

8 CHEN, Y.-H. et al. Accelerated and noise-resistant generation of high-fidelity steady-state entanglement with rydberg atoms. *Phys. Rev. A*, American Physical Society, v. 97, p. 032328, Mar 2018. Disponível em: <https://link.aps.org/doi/10.1103/PhysRevA.97.032328>.

9 WU, J.-L.; SONG, J.; SU, S.-L. Resonant-interaction-induced rydberg antiblockade and its applications. *Physics Letters A*, v. 384, n. 1, p. 126039, 2020. ISSN 0375-9601. Disponível em: <https://www.sciencedirect.com/science/article/pii/S0375960119309223>.

10 SU, S.-L. et al. Applications of the modified rydberg antiblockade regime with simultaneous driving. *Phys. Rev. A*, American Physical Society, v. 96, p. 042335, Oct 2017. Disponível em: <https://link.aps.org/doi/10.1103/PhysRevA.96.042335>.

11 ANDERSON, W. R.; VEALE, J. R.; GALLAGHER, T. F. Resonant dipole-dipole energy transfer in a nearly frozen rydberg gas. *Phys. Rev. Lett.*, American Physical Society, v. 80, p. 249–252, Jan 1998. Disponível em: <https://link.aps.org/doi/10.1103/PhysRevLett.80.249>.

12 DITZHUIJZEN, C. S. E. van et al. Spatially resolved observation of dipole-dipole interaction between rydberg atoms. *Phys. Rev. Lett.*, American Physical Society, v. 100, p.

243201, Jun 2008. Disponível em: <https://link.aps.org/doi/10.1103/PhysRevLett.100.243201>.

13 MOURACHKO, I. et al. Many-body effects in a frozen rydberg gas. *Phys. Rev. Lett.*, American Physical Society, v. 80, p. 253–256, Jan 1998. Disponível em: <https://link.aps.org/doi/10.1103/PhysRevLett.80.253>.

14 MÜLKEN, O. et al. Survival probabilities in coherent exciton transfer with trapping. *Phys. Rev. Lett.*, American Physical Society, v. 99, p. 090601, Aug 2007. Disponível em: <https://link.aps.org/doi/10.1103/PhysRevLett.99.090601>.

15 GREENE, C. H.; DICKINSON, A. S.; SADEGHPOUR, H. R. Creation of polar and nonpolar ultra-long-range rydberg molecules. *Phys. Rev. Lett.*, American Physical Society, v. 85, p. 2458–2461, Sep 2000. Disponível em: <https://link.aps.org/doi/10.1103/PhysRevLett.85.2458>.

16 BOISSEAU, C.; SIMBOTIN, I.; CÔTÉ, R. Macrodimers: Ultralong range rydberg molecules. *Phys. Rev. Lett.*, American Physical Society, v. 88, p. 133004, Mar 2002. Disponível em: <https://link.aps.org/doi/10.1103/PhysRevLett.88.133004>.

17 GALLAGHER, T. Rydberg atoms. In: _____. *Springer Handbook of Atomic, Molecular, and Optical Physics*. New York, NY: Springer New York, 2006. p. 235–245. ISBN 978-0-387-26308-3. Disponível em: <https://doi.org/10.1007/978-0-387-26308-3_14>.

18 SAFFMAN, M.; WALKER, T. G.; MØLMER, K. Quantum information with rydberg atoms. *Rev. Mod. Phys.*, American Physical Society, v. 82, p. 2313–2363, Aug 2010. Disponível em: <https://link.aps.org/doi/10.1103/RevModPhys.82.2313>.

19 VALLE, E. del et al. Theory of frequency-filtered and time-resolved n-photon correlations. *Phys. Rev. Lett.*, American Physical Society, v. 109, p. 183601, Oct 2012. Disponível em: <https://link.aps.org/doi/10.1103/PhysRevLett.109.183601>.

20 VALLE, E. del. Distilling one, two and entangled pairs of photons from a quantum dot with cavity QED effects and spectral filtering. *New Journal of Physics*, IOP Publishing, v. 15, n. 2, p. 025019, feb 2013. Disponível em: <https://doi.org/10.1088/1367-2630/15/2/025019>.

21 DARSHESHDAR, E. et al. Photon-photon correlations from a pair of strongly coupled two-level emitters. *Phys. Rev. A*, American Physical Society, v. 103, p. 053702, May 2021. Disponível em: <https://link.aps.org/doi/10.1103/PhysRevA.103.053702>.

22 CARREñO, J.; VALLE, E. del; LAUSSY, F. Photon correlations from the mollow triplet. *Laser Photonics Rev.*, Willey VCH, v. 11, p. 1–10, Aug 2017. Disponível em: <https://onlinelibrary.wiley.com/doi/abs/10.1002/lpor.201700090>.

23 NOZ, C. S. M. et al. Violation of classical inequalities by photon frequency filtering. *Phys. Rev. A*, American Physical Society, v. 90, p. 052111, Nov 2014. Disponível em: <https://link.aps.org/doi/10.1103/PhysRevA.90.052111>.

24 GONZALEZ-TUDELA, A. et al. Two-photon spectra of quantum emitters. *New Journal of Physics*, IOP Publishing, v. 15, n. 3, p. 033036, mar 2013. Disponível em: <https://doi.org/10.1088/1367-2630/15/3/033036>.

25 SCULLY M.O., Z. M. *Quantum optics*. [S.l.]: Cambridge University Press, 1997.

26 Eisberg, R.; Resnick, R. *Quantum Physics of Atoms, Molecules, Solids, Nuclei, and Particles, 2nd Edition*. [S.l.: s.n.], 1985.

27 LOUDON, R. *The Quantum Theory of Light*. [S.l.]: Oxford Science Publications, 2001.

28 ḡLU, A. Imamoet al. Strongly interacting photons in a nonlinear cavity. *Phys. Rev. Lett.*, American Physical Society, v. 79, p. 1467–1470, Aug 1997. Disponível em: <https://link.aps.org/doi/10.1103/PhysRevLett.79.1467>.

29 BIRNBAUM, K. et al. Photon blockade in an optical cavity with one trapped atom. *Nature*, Springer Science and Business Media LLC, p. 87–90, jul 2005. Disponível em: <https://www.nature.com/articles/nature03804>.

30 RABL, P. Photon blockade effect in optomechanical systems. *Phys. Rev. Lett.*, American Physical Society, v. 107, p. 063601, Aug 2011. Disponível em: <https://link.aps.org/doi/10.1103/PhysRevLett.107.063601>.

31 HUANG, J.-F.; LIAO, J.-Q.; SUN, C. P. Photon blockade induced by atoms with rydberg coupling. *Phys. Rev. A*, American Physical Society, v. 87, p. 023822, Feb 2013. Disponível em: <https://link.aps.org/doi/10.1103/PhysRevA.87.023822>.

32 URBAN, E. et al. Observation of rydberg blockade between two atoms. *Nature*, Springer Science and Business Media LLC, v. 5, p. 110–114, jan 2009. Disponível em: <https://www.nature.com/articles/nphys1178#citeas>.

33 GAëTAN, A. et al. Observation of collective excitation of two individual atoms in the rydberg blockade regime. *Nature*, Springer Science and Business Media LLC, v. 5, p. 115–118, jan 2009. Disponível em: <https://www.nature.com/articles/nphys1183#citeas>.

34 WILLIAMSON, L. A.; BORGH, M. O.; RUOSTEKOSKI, J. Superatom picture of collective nonclassical light emission and dipole blockade in atom arrays. *Phys. Rev. Lett.*, American Physical Society, v. 125, p. 073602, Aug 2020. Disponível em: <https://link.aps.org/doi/10.1103/PhysRevLett.125.073602>.

35 WANG, Y. et al. Dark state optical lattice with a subwavelength spatial structure. *Phys. Rev. Lett.*, American Physical Society, v. 120, p. 083601, Feb 2018. Disponível em: <https://link.aps.org/doi/10.1103/PhysRevLett.120.083601>.

36 SUBHANKAR, S. et al. Floquet engineering of optical lattices with spatial features and periodicity below the diffraction limit. *New Journal of Physics*, IOP Publishing, v. 21, n. 11, p. 113058, nov 2019. Disponível em: <https://doi.org/10.1088/1367-2630/ab500f>.

37 TSUI, T.-C. et al. Realization of a stroboscopic optical lattice for cold atoms with subwavelength spacing. *Phys. Rev. A*, American Physical Society, v. 101, p. 041603, Apr 2020. Disponível em: <https://link.aps.org/doi/10.1103/PhysRevA.101.041603>.

38 ATES, C. et al. Antiblockade in rydberg excitation of an ultracold lattice gas. *Phys. Rev. Lett.*, American Physical Society, v. 98, p. 023002, Jan 2007. Disponível em: <https://link.aps.org/doi/10.1103/PhysRevLett.98.023002>.

39 AMTHOR, T. et al. Evidence of antiblockade in an ultracold rydberg gas. *Phys. Rev. Lett.*, American Physical Society, v. 104, p. 013001, Jan 2010. Disponível em: <https://link.aps.org/doi/10.1103/PhysRevLett.104.013001>.

40 LI, W.; ATES, C.; LESANOVSKY, I. Nonadiabatic motional effects and dissipative blockade for rydberg atoms excited from optical lattices or microtraps. *Phys. Rev. Lett.*, American Physical Society, v. 110, p. 213005, May 2013. Disponível em: <https://link.aps.org/doi/10.1103/PhysRevLett.110.213005>.

41 TAYLOR, J. et al. *Generation of doubly excited Rydberg states based on Rydberg antiblockade in a cold atomic ensemble*. 2019.

42 LEHMBERG, R. H. Radiation from an n-atom system. i. general formalism. *Phys. Rev. A*, American Physical Society, v. 2, p. 883–888, Sep 1970. Disponível em: <https://link.aps.org/doi/10.1103/PhysRevA.2.883>.

43 STEPHEN, M. J. First-order dispersion forces. *The Journal of Chemical Physics*, v. 40, n. 3, p. 669–673, 1964. Disponível em: <https://doi.org/10.1063/1.1725188>.

44 STECK, D. *Quantum and Atom Optics*. [s.n.], 2020. Disponível em: <https://atomoptics.uoregon.edu/~dsteck/teaching/quantum-optics/>.

45 JACKSON, J. D. *Classical Electrodynamics*. [S.l.]: John Wiley and Sons, Inc., 1999.

46 FRIEDBERG, R.; MANASSAH, J. T. Analytic expressions for the initial cooperative decay rate and cooperative lamb shift for a spherical sample of two-level atoms. *Physics Letters A*, v. 374, n. 15, p. 1648–1659, 2010. ISSN 0375-9601. Disponível em: <https://www.sciencedirect.com/science/article/pii/S0375960110001726>.

47 SCULLY, M. O. et al. Directed spontaneous emission from an extended ensemble of n atoms: Timing is everything. *Phys. Rev. Lett.*, American Physical Society, v. 96, p. 010501, Jan 2006. Disponível em: <https://link.aps.org/doi/10.1103/PhysRevLett.96.010501>.

48 GUERIN, W.; ARAÚJO, M. O.; KAISER, R. Subradiance in a large cloud of cold atoms. *Phys. Rev. Lett.*, American Physical Society, v. 116, p. 083601, Feb 2016. Disponível em: <https://link.aps.org/doi/10.1103/PhysRevLett.116.083601>.

49 GOETSCHY, A.; SKIPETROV, S. E. Non-hermitian euclidean random matrix theory. *Phys. Rev. E*, American Physical Society, v. 84, p. 011150, Jul 2011. Disponível em: <https://link.aps.org/doi/10.1103/PhysRevE.84.011150>.

50 BELLANDO, L. et al. Cooperative effects and disorder: A scaling analysis of the spectrum of the effective atomic hamiltonian. *Phys. Rev. A*, American Physical Society, v. 90, p. 063822, Dec 2014. Disponível em: <https://link.aps.org/doi/10.1103/PhysRevA.90.063822>.

51 VOGEL, W.; WELSCH, D.-G. *Quantum optics*. [S.l.]: John Wiley & Sons, 2006.

52 MOLLOW, B. R. Power spectrum of light scattered by two-level systems. *Phys. Rev.*, American Physical Society, v. 188, p. 1969–1975, Dec 1969. Disponível em: <https://link.aps.org/doi/10.1103/PhysRev.188.1969>.

53 SCHUDA, F.; STROUD, C. R.; HERCHER, M. Observation of the resonant stark effect at optical frequencies. *Journal of Physics B: Atomic and Molecular Physics*, IOP Publishing, v. 7, n. 7, p. L198–L202, may 1974. Disponível em: <https://doi.org/10.1088/0022-3700/7/7/002>.

54 BIENERT, M. et al. Resonance fluorescence of a cold atom in a high-finesse resonator. *Phys. Rev. A*, American Physical Society, v. 76, p. 013410, Jul 2007. Disponível em: <https://link.aps.org/doi/10.1103/PhysRevA.76.013410>.

55 FAGG, E. et al. Resonantly driven coherent oscillations in a solid-state quantum emitter. *Nat. Phys*, Springer Science and Business Media LLC, v. 5, p. 203–207, jan 2009. Disponível em: <https://www.nature.com/articles/nphys1184#citeas>.

56 ASTAFIEV, O. et al. Resonance fluorescence of a single artificial atom. *Science*, v. 327, n. 5967, p. 840–843, 2010. Disponível em: <https://www.science.org/doi/abs/10.1126/science.1181918>.

57 COHEN-TANNOUDJI, C.; REYNAUD, S. Dressed-atom description of resonance fluorescence and absorption spectra of a multi-level atom in an intense laser beam. *Journal of Physics B: Atomic and Molecular Physics*, IOP Publishing, v. 10, n. 3, p. 345–363, feb 1977. Disponível em: <https://doi.org/10.1088/0022-3700/10/3/005>.

58 APANASEVICH, P. A.; KILIN, S. J. Photon bunching and antibunching in resonance fluorescence. *Journal of Physics B: Atomic and Molecular Physics*, IOP Publishing, v. 12, n. 3, p. L83–L86, feb 1979. Disponível em: <https://doi.org/10.1088/0022-3700/12/3/003>.

59 COHEN-TANNOUDJI, C. et al. Atoms in strong light-fields: photon antibunching in single atom fluorescence. *Philosophical Transactions of the Royal Society of London. Series A, Mathematical and Physical Sciences*, v. 293, n. 1402, p. 223–237, 1979. Disponível em: <https://royalsocietypublishing.org/doi/abs/10.1098/rsta.1979.0092>.

60 ASPECT, A. et al. Time correlations between the two sidebands of the resonance fluorescence triplet. *Phys. Rev. Lett.*, American Physical Society, v. 45, p. 617–620, Aug 1980. Disponível em: <https://link.aps.org/doi/10.1103/PhysRevLett.45.617>.

61 AL-HILFY, A.; LOUDON, R. Theory of photon correlations in two-photon cascade emission. *Journal of Physics B: Atomic and Molecular Physics*, IOP Publishing, v. 18, n. 18, p. 3697–3712, sep 1985. Disponível em: <https://doi.org/10.1088/0022-3700/18/18/011>.

62 ARNOLDUS, H. F.; NIENHUIS, G. Photon correlations between the lines in the spectrum of resonance fluorescence. *Journal of Physics B: Atomic and Molecular Physics*, IOP Publishing, v. 17, n. 6, p. 963–977, mar 1984. Disponível em: <https://doi.org/10.1088/0022-3700/17/6/011>.

63 KNOLL, L.; WEBER, G.; SCHAFER, T. Theory of time-resolved correlation spectroscopy and its application to resonance fluorescence radiation. *Journal of Physics B: Atomic and Molecular Physics*, IOP Publishing, v. 17, n. 24, p. 4861–4875, dec 1984. Disponível em: <https://doi.org/10.1088/0022-3700/17/24/020>.

64 NIENHUIS, G. Spectral correlations in resonance fluorescence. *Phys. Rev. A*, American Physical Society, v. 47, p. 510–518, Jan 1993. Disponível em: <https://link.aps.org/doi/10.1103/PhysRevA.47.510>.

65 ASPECT, A.; GRANGIER, P.; ROGER, G. Experimental tests of realistic local theories via bell's theorem. *Phys. Rev. Lett.*, American Physical Society, v. 47, p. 460–463, Aug 1981. Disponível em: <https://link.aps.org/doi/10.1103/PhysRevLett.47.460>.

66 ASPECT, A.; DALIBARD, J.; ROGER, G. Experimental test of bell's inequalities using time-varying analyzers. *Phys. Rev. Lett.*, American Physical Society, v. 49, p. 1804–1807, Dec 1982. Disponível em: <https://link.aps.org/doi/10.1103/PhysRevLett.49.1804>.

67 PEIRIS, M. et al. Two-color photon correlations of the light scattered by a quantum dot. *Phys. Rev. B*, American Physical Society, v. 91, p. 195125, May 2015. Disponível em: <https://link.aps.org/doi/10.1103/PhysRevB.91.195125>.

68 ZBILUT, J. P.; MARWAN, N. The wiener–khinchin theorem and recurrence quantification. *Physics Letters A*, v. 372, n. 44, p. 6622–6626, 2008. ISSN 0375-9601. Disponível em: <https://www.sciencedirect.com/science/article/pii/S0375960108014102>.

69 EBERLY, J. H.; WóDKIEWICZ, K. The time-dependent physical spectrum of light∗. *J. Opt. Soc. Am.*, OSA, v. 67, n. 9, p. 1252–1261, Sep 1977. Disponível em: <http://opg.optica.org/abstract.cfm?URI=josa-67-9-1252>.

70 KNöLL, L.; VOGEL, W.; WELSCH, D.-G. Quantum noise in spectral filtering of light. *J. Opt. Soc. Am. B*, OSA, v. 3, n. 10, p. 1315–1318, Oct 1986. Disponível em: <http://opg.optica.org/josab/abstract.cfm?URI=josab-3-10-1315>.

71 CRESSER, J. D. Intensity correlations of frequency-filtered light fields. *Journal of Physics B: Atomic and Molecular Physics*, IOP Publishing, v. 20, n. 18, p. 4915–4927, sep 1987. Disponível em: <https://doi.org/10.1088/0022-3700/20/18/027>.

72 JOOSTEN, K.; NIENHUIS, G. Influence of spectral filtering on the quantum nature of light. *Journal of Optics B: Quantum and Semiclassical Optics*, IOP Publishing, v. 2, n. 2, p. 158–164, apr 2000. Disponível em: <https://doi.org/10.1088/1464-4266/2/2/317>.

73 LOUDON, R. Non-classical effects in the statistical properties of light. *Reports on Progress in Physics*, IOP Publishing, v. 43, n. 7, p. 913–949, jul 1980. Disponível em: <https://doi.org/10.1088/0034-4885/43/7/002>.

74 BELL, J. S. On the problem of hidden variables in quantum mechanics. *Rev. Mod. Phys.*, American Physical Society, v. 38, p. 447–452, Jul 1966. Disponível em: <https://link.aps.org/doi/10.1103/RevModPhys.38.447>.

75 REID, M. D.; WALLS, D. F. Violations of classical inequalities in quantum optics. *Phys. Rev. A*, American Physical Society, v. 34, p. 1260–1276, Aug 1986. Disponível em: <https://link.aps.org/doi/10.1103/PhysRevA.34.1260>.

76 CLAUSER, J. F. Experimental distinction between the quantum and classical field-theoretic predictions for the photoelectric effect. *Phys. Rev. D*, American Physical Society, v. 9, p. 853–860, Feb 1974. Disponível em: <https://link.aps.org/doi/10.1103/PhysRevD.9.853>.

77 THOMPSON, J. K. et al. A high-brightness source of narrowband, identical-photon pairs. *Science*, v. 313, n. 5783, p. 74–77, 2006. Disponível em: <https://www.science.org/doi/abs/10.1126/science.1127676>.

78 SRIVATHSAN, B. et al. Narrow band source of transform-limited photon pairs via four-wave mixing in a cold atomic ensemble. *Phys. Rev. Lett.*, American Physical Society, v. 111, p. 123602, Sep 2013. Disponível em: <https://link.aps.org/doi/10.1103/PhysRevLett.111.123602>.

79 JOHANSSON, J.; NATION, P.; NORI, F. Qutip: An open-source python framework for the dynamics of open quantum systems. *Computer Physics Communications*, v. 183, n. 8, p. 1760–1772, 2012. ISSN 0010-4655. Disponível em: <https://www.sciencedirect.com/science/article/pii/S0010465512000835>.

80 JOHANSSON, J.; NATION, P.; NORI, F. Qutip 2: A python framework for the dynamics of open quantum systems. *Computer Physics Communications*, v. 184, n. 4, p. 1234–1240, 2013. ISSN 0010-4655. Disponível em: <https://www.sciencedirect.com/science/article/pii/S0010465512003955>.

81 COMPAGNO, G.; PASSANTE, R.; PERSICO, F. Atoms dressed by a real e.m. field. In: _____. *Atom-Field Interactions and Dressed Atoms*. [S.l.]: Cambridge University Press, 1995. (Cambridge Studies in Modern Optics), p. 114–158.

82 PHILLIPS, C. L. et al. Photon statistics of filtered resonance fluorescence. *Phys. Rev. Lett.*, American Physical Society, v. 125, p. 043603, Jul 2020. Disponível em: <https://link.aps.org/doi/10.1103/PhysRevLett.125.043603>.

83 CARMICHAEL, H. *An Open Systems Approach to Quantum Optics*. [S.l.]: Springer - Verlag, 1991.

84 ATTAL, S.; JOYCE, A.; PILLET, C.-A. *Open Quantum Systems I: The Hamiltonian Approach*. [S.l.]: Springer, 2003.

85 KOSSAKOWSKI, A. On quantum statistical mechanics of non-hamiltonian systems. *Reports on Mathematical Physics*, v. 3, n. 4, p. 247–274, 1972. ISSN 0034-4877. Disponível em: <https://www.sciencedirect.com/science/article/pii/0034487772900109>.

86 MOY, G. M.; HOPE, J. J.; SAVAGE, C. M. Born and markov approximations for atom lasers. *Phys. Rev. A*, American Physical Society, v. 59, p. 667–675, Jan 1999. Disponível em: <https://link.aps.org/doi/10.1103/PhysRevA.59.667>.

87 WILDE, M. *Quantum Information Theory*. [S.l.]: Cambridge University Press, 2013.

A Second-order correlation function for two atoms

We can see in Figs. 4(a) and 4(b) that the plot of P_2/P_1^2 is identical to the $g^{(2)}(0)$ plot. Indeed, we can demonstrate that $g^{(2)}(0) = P_2/P_1^2$ for a two-atom system. From equation (2.11), we have the following expression for $g^{(2)}(0)$:

$$g^{(2)}(0) = \lim_{t\to\infty} \frac{\langle \hat{E}^-(t)\hat{E}^-(t)\hat{E}^+(t)\hat{E}^+(t)\rangle}{\langle \hat{E}^-(t)\hat{E}^+(t)\rangle^2}. \tag{A.1}$$

We are considering the far-field approximation and the steady-state regime in this work, so we can write the electric field operator as follows:

$$\hat{E}^{\pm} \approx \sum_{i=1}^{N} \hat{\sigma}_i^{\pm}, \tag{A.2}$$

where N is the number of atoms and $\hat{\sigma}_i^{\pm}$ is the rising/lowering atomic operator. For $N = 2$:

$$\hat{E^+} = \hat{\sigma}_1^- + \hat{\sigma}_2^-, \tag{A.3}$$

$$\hat{E^-} = \hat{\sigma}_1^+ + \hat{\sigma}_2^+. \tag{A.4}$$

Using these results, we can calculate the term $\hat{E}^-(t)\hat{E}^-(t)\hat{E}^+(t)\hat{E}^+(t)$:

$$\begin{aligned}
\hat{E}^-(t)\hat{E}^-(t)\hat{E}^+(t)\hat{E}^+(t) &= (\hat{\sigma}_1^+ + \hat{\sigma}_2^+)(\hat{\sigma}_1^+ + \hat{\sigma}_2^+)(\hat{\sigma}_1^- + \hat{\sigma}_2^-)(\hat{\sigma}_1^- + \hat{\sigma}_2^-) \\
&= \hat{\sigma}_1^+\hat{\sigma}_1^+\hat{\sigma}_1^-\hat{\sigma}_1^- + \hat{\sigma}_1^+\hat{\sigma}_1^+\hat{\sigma}_1^-\hat{\sigma}_2^- + \hat{\sigma}_1^+\hat{\sigma}_1^+\hat{\sigma}_2^-\hat{\sigma}_1^- + \hat{\sigma}_1^+\hat{\sigma}_1^+\hat{\sigma}_2^-\hat{\sigma}_2^- \\
&+ \hat{\sigma}_1^+\hat{\sigma}_2^+\hat{\sigma}_1^-\hat{\sigma}_1^- + \hat{\sigma}_1^+\hat{\sigma}_2^+\hat{\sigma}_1^-\hat{\sigma}_2^- + \hat{\sigma}_1^+\hat{\sigma}_2^+\hat{\sigma}_2^-\hat{\sigma}_1^- + \hat{\sigma}_1^+\hat{\sigma}_2^+\hat{\sigma}_2^-\hat{\sigma}_2^- \\
&+ \hat{\sigma}_2^+\hat{\sigma}_1^+\hat{\sigma}_1^-\hat{\sigma}_1^- + \hat{\sigma}_2^+\hat{\sigma}_1^+\hat{\sigma}_1^-\hat{\sigma}_2^- + \hat{\sigma}_2^+\hat{\sigma}_1^+\hat{\sigma}_2^-\hat{\sigma}_1^- + \hat{\sigma}_2^+\hat{\sigma}_1^+\hat{\sigma}_2^-\hat{\sigma}_2^- \\
&+ \hat{\sigma}_2^+\hat{\sigma}_2^+\hat{\sigma}_1^-\hat{\sigma}_1^- + \hat{\sigma}_2^+\hat{\sigma}_2^+\hat{\sigma}_1^-\hat{\sigma}_2^- + \hat{\sigma}_2^+\hat{\sigma}_2^+\hat{\sigma}_2^-\hat{\sigma}_1^- + \hat{\sigma}_2^+\hat{\sigma}_2^+\hat{\sigma}_2^-\hat{\sigma}_2^-.
\end{aligned} \tag{A.5}$$

The atomic operators have the following form:

$$\hat{\sigma}_1^+ = (|\uparrow\rangle\langle\uparrow|)_1 \otimes \mathbb{I}_2, \tag{A.6}$$

$$\hat{\sigma}_2^+ = \mathbb{I}_1 \otimes (|\uparrow\rangle\langle\uparrow|)_2, \tag{A.7}$$

$$\hat{\sigma}_1^- = (|\downarrow\rangle\langle\uparrow|)_1 \otimes \mathbb{I}_2, \tag{A.8}$$

$$\hat{\sigma}_2^- = \mathbb{I}_1 \otimes (|\downarrow\rangle\langle\uparrow|)_2. \tag{A.9}$$

Considering the tensorial product property: $(\mathbf{v}\otimes\mathbf{w})(\mathbf{x}\otimes\mathbf{y}) = \mathbf{vx}\otimes\mathbf{wy}$, we can obtain:

$$\hat{\sigma}_1^+\hat{\sigma}_1^+ = \hat{\sigma}_1^-\hat{\sigma}_1^- = \hat{\sigma}_2^+\hat{\sigma}_2^+ = \hat{\sigma}_2^-\hat{\sigma}_2^- = 0,$$

which allows us to simplify equation (A.5) into:

$$\hat{E}^-(t)\hat{E}^-(t)\hat{E}^+(t)\hat{E}^+(t) = \hat{\sigma}_1^+\hat{\sigma}_2^+\hat{\sigma}_1^-\hat{\sigma}_2^- + \hat{\sigma}_1^+\hat{\sigma}_2^+\hat{\sigma}_2^-\hat{\sigma}_1^- + \hat{\sigma}_2^+\hat{\sigma}_1^+\hat{\sigma}_1^-\hat{\sigma}_2^- + \hat{\sigma}_2^+\hat{\sigma}_1^+\hat{\sigma}_2^-\hat{\sigma}_1^-, \tag{A.10}$$

where:

$$\hat{\sigma}_1^+\hat{\sigma}_2^+\hat{\sigma}_2^+\hat{\sigma}_1^+ = |\uparrow\uparrow\rangle\langle\downarrow\downarrow|, \tag{A.11}$$

$$\hat{\sigma}_1^-\hat{\sigma}_2^- = \hat{\sigma}_2^-\hat{\sigma}_1^- = |\downarrow\downarrow\rangle\langle\uparrow\uparrow|. \tag{A.12}$$

Then, equation (A.10) can be rewritten as:

$$\hat{E}^-(t)\hat{E}^-(t)\hat{E}^+(t)\hat{E}^+(t) = 4\,|\uparrow\uparrow\rangle\langle\downarrow\downarrow|, \tag{A.13}$$

$$\hat{E}^-(t)\hat{E}^-(t)\hat{E}^+(t)\hat{E}^+(t) = 4\hat{P}_2, \tag{A.14}$$

where $\hat{P}_2$ is the projector over the two-excitation manifold. Following the same procedure for the term $\hat{E}^-(t)\hat{E}^+(t)$ in equation (A.1), we obtain:

$$\hat{E}^-(t)\hat{E}^+(t) = (|\uparrow\rangle\langle\uparrow|)_1 \otimes \mathbb{I}_2 + \mathbb{I}_1 \otimes (|\uparrow\rangle\langle\uparrow|)_2 = \hat{P}_1 + \hat{P}_1 = 2\hat{P}_1, \tag{A.15}$$

where $\hat{P}_1$ is the projector over the single-excitation manifold.

Substituting (A.14) and (A.15) in (A.1):

$$g^{(2)}(0) = \frac{4\langle\hat{P}_2\rangle}{\langle 2\hat{P}_1\rangle^2} = \frac{\langle\hat{P}_2\rangle}{\langle\hat{P}_1\rangle^2}, \tag{A.16}$$

with $\langle\hat{P}_2\rangle = P_2$ (population in the two-excitation manifold) and $\langle\hat{P}_1\rangle = P_1$ (population in the single-excitation manifold), we finally show that:

$$g^{(2)}(0) = \frac{P_2}{P_1^2}. \tag{A.17}$$

B Master Equation in the Born-Markov approximation

A considerable part of the works in quantum optics involves light sources that emit photons irreversibly (photoemissive sources): the photons propagate until they are absorbed by a boundary of the system (the laboratory wall, for example) or by the detectors associated with the system. Let us compare this situation with the following: an electromagnetic field confined within a perfect cavity and measured by detectors inside the cavity. In the first situation, the detectors do not interact directly with the source, since the photons already left it in an irreversibly way. But in the second situation, the detectors interact with the source, and the description of the dynamics of the field when the detectors are present is quite different [83].

In this work, we will consider a system with a number of two-level atoms interacting with each other and with a radiation field, and where the atomic system behaves as a photoemissive source. Such a system is classified as an open quantum system [84], precisely because it interacts with the environment (usually referred to as a reservoir or bath). Indeed, it is possible to eliminate the photonic dynamics and build an equation for the effective atomic dynamics, under the form of a master equation [85].

The evolution of the atomic system plus reservoir is described by the following Hamiltonian:

$$\hat{H} = \hat{H}_S + \hat{H}_R + \hat{H}_{RS}, \tag{B.1}$$

where $\hat{H}_S$, $\hat{H}_R$ and $\hat{H}_{RS}$ refer, respectively, to the atomic system, reservoir, and atomic system-reservoir coupling. The state of the interaction atomic system-reservoir is described by the density matrix ρ_{RS}, whose evolution is given by the Schrödinger-von Neumann equation [44]:

$$\partial_t \hat{\rho}_{RS} = -\frac{i}{\hbar}\left[\hat{H}_{RS}, \hat{\rho}_{RS}\right], \tag{B.2}$$

If we move to the interaction picture, the following transformations [44] must be done:

$$\hat{\rho}'_{RS} = e^{i(\hat{H}_S+\hat{H}_R)t/\hbar}\hat{\rho}_{RS}(t)e^{-i(\hat{H}_S+\hat{H}_R)t/\hbar}, \tag{B.3}$$

$$\hat{H}'_{RS} = e^{i(\hat{H}_S+\hat{H}_R)t/\hbar}\hat{H}_{RS}(t)e^{-i(\hat{H}_S+\hat{H}_R)t/\hbar}, \tag{B.4}$$

then the equation of motion in this picture reads:

$$\partial_t \hat{\rho}'_{RS}(t) = -\frac{i}{\hbar}\left[\hat{H}'_{RS}(t), \hat{\rho}'_{RS}(t)\right]. \tag{B.5}$$

Integrating equation (B.5) from t to $t+\Delta t$ we obtain:

$$\int_t^{t+\Delta t} \partial_{t'} \hat{\rho}'_{RS}(t')dt' = -\frac{i}{\hbar}\int_t^{t+\Delta t} \left[\hat{H}'_{RS}(t'), \hat{\rho}'_{RS}(t')\right] dt',$$

$$\hat{\rho}'_{RS}(t+\Delta t) - \hat{\rho}'_{RS}(t) = -\frac{i}{\hbar}\int_t^{t+\Delta t} \left[\hat{H}'_{RS}(t'), \hat{\rho}'_{RS}(t')\right] dt'. \tag{B.6}$$

where t is an arbitrary instant of time, and $\Delta t = t' - t$ is the smallest time-scale of the system-reservoir interaction dynamics. Iterating equation (B.6), given that $\hat{\rho}'_{RS}(t')$ must satisfy equation (B.5), so:

$$\hat{\rho}'_{RS}(t') = \hat{\rho}'_{RS}(t) - \frac{i}{\hbar}\int_t^{t'} \left[\hat{H}'_{RS}(t''), \hat{\rho}'_{RS}(t'')\right] dt'', \tag{B.7}$$

and substituting Eq. (B.7) in Eq. (B.6) leads us to the following result:

$$\hat{\rho}'_{RS}(t+\Delta t) - \hat{\rho}'_{RS}(t) = -\frac{i}{\hbar}\int_t^{t+\Delta t} dt' \left[\hat{H}'_{RS}(t'), \hat{\rho}'_{RS}(t) - \frac{i}{\hbar}\int_t^{t'} \left[\hat{H}'_{RS}(t''), \hat{\rho}'_{RS}(t'')\right] dt''\right]. \tag{B.8}$$

The term in the integrand of equation (B.8) can be rewritten as:

$$\begin{aligned}\hat{\rho}'_{RS}(t+\Delta t) - \hat{\rho}'_{RS}(t) = \Delta\hat{\rho}'_{RS}(t) = -\frac{i}{\hbar}\int_t^{t+\Delta t} \left[\hat{H}'_{RS}(t'), \hat{\rho}'_{RS}(t)\right] dt' \\ -\frac{1}{\hbar^2}\int_t^{t+\Delta t} dt' \int_t^{t'} \left[\hat{H}'_{RS}(t'), \left[\hat{H}'_{RS}(t''), \hat{\rho}'_{RS}(t'')\right]\right] dt''.\end{aligned} \tag{B.9}$$

Here we consider that the perturbation of the reservoir over the system is weak, which allows us to use the Born approximation: the state of the reservoir does not significantly change due to the interaction with the system and remains separable throughout the evolution [86]. We can thus neglect higher-order terms in the time expansion above, and thus neglect further iterations in Eq. (B.8).

Since the system and reservoir are weakly coupled, the Hamiltonian of the interaction between them can be written as a sum of products over system operators $\hat{S}$ and reservoir operators $\hat{R}$, as expressed in the equation below:

$$\hat{H}'_{RS} = \hbar\hat{S}'_\alpha\hat{R}'_\alpha. \tag{B.10}$$

We have here used the Einstein notation, where repeated indices imply summation, i.e., $\hat{S}'_\alpha\hat{R}'_\alpha = \sum_\alpha \hat{S}'_\alpha\hat{R}'_\alpha$.

We will consider now the following change of variable in the integrals of Eq. (B.9):

$$\tau = t' - t'', \tag{B.11}$$

which implies that:

$$\int_t^{t+\Delta t} dt' \int_t^{t'} dt'' = \int_0^{\Delta t} d\tau \int_t^{t+\Delta t} dt'. \tag{B.12}$$

Here τ is the time scale of decay for the reservoir, which is assumed to be much shorter than the smallest time scale of the system Δt. This consideration ($\tau \ll \Delta t$) is called the Markov approximation [86] and it implies a short memory for the reservoir, which means that the correlations in the reservoir decay much faster than the system correlations.

Combining Eqs. (B.12) and (B.9), we obtain:

$$\begin{aligned}\Delta\hat{\rho}'_{RS}(t) = &-\frac{i}{\hbar}\int_t^{t+\Delta t}\left[\hat{H}'_{RS}(t'),\hat{\rho}'_{RS}(t)\right]dt' \\ &-\frac{1}{\hbar^2}\int_0^{\Delta t}d\tau\int_t^{t+\Delta t}dt'\left[\hat{H}'_{RS}(t'),\left[\hat{H}'_{RS}(t'-\tau),\hat{\rho}'_{RS}(t'-\tau)\right]\right],\end{aligned} \tag{B.13}$$

and substituting Eq. (B.10) in Eq. (B.13):

$$\begin{aligned}\Delta\hat{\rho}'_{RS}(t) = &-\frac{i}{\hbar}\int_t^{t+\Delta t}\hbar\left[\hat{S}'_\alpha(t')\hat{R}'_\alpha(t'),\hat{\rho}'(t)\right]dt \\ &-\int_0^{\Delta t}d\tau\int_t^{t+\Delta t}dt'\Big[\hat{S}'_\alpha(t')\hat{S}'_\beta(t'-\tau)\hat{\rho}'_{RS}(t)-\hat{S}'_\beta(t'-\tau)\hat{\rho}'_{RS}(t)\hat{S}'_\alpha(t')\Big]\hat{R}_\alpha(t')\hat{R}_\beta(t'-\tau) \\ &+\Big[\hat{\rho}'_{RS}(t)\hat{S}'_\beta(t'-\tau)\hat{S}'_\alpha(t')-\hat{S}'_\alpha(t')\hat{\rho}'_{RS}(t)\hat{S}'_\beta(t'-\tau)\Big]\hat{R}_\beta(t'-\tau)\hat{R}_\alpha(t').\end{aligned} \tag{B.14}$$

Assuming that $\hat{S}'_\alpha(t')$ commutes with $\hat{\rho}'_S(t)$, i.e., $\left[\hat{S}'_\alpha(t'),\hat{\rho}'_S(t)\right]=0$, and using the invariant property of the partial trace [87],we have:

$$Tr_R\left[\hat{S}'_\alpha(t')\hat{R}'_\alpha(t'),\hat{\rho}'(t)\right]=0, \tag{B.15}$$

$$\begin{aligned}Tr_R\Big[\Big(\hat{S}'_\alpha(t')\hat{S}'_\beta(t'-\tau)\hat{\rho}'_{RS}(t)-\hat{S}'_\beta(t'-\tau)\hat{\rho}'_{RS}(t)\hat{S}'_\alpha(t')\Big)\hat{R}_\alpha(t')\hat{R}_\beta(t'-\tau)\Big)\Big] = \\ \Big[\hat{S}'_\alpha(t')\hat{S}'_\beta(t'-\tau)\hat{\rho}'_S(t)-\hat{S}'_\beta(t'-\tau)\hat{\rho}'_S(t)\hat{S}'_\alpha(t')\Big],\end{aligned} \tag{B.16}$$

$$Tr_R[\Delta\hat{\rho}'_{RS}(t)]=\Delta\rho'_S(t). \tag{B.17}$$

Then Eq. (B.14) becomes:

$$\begin{aligned}\Delta\hat{\rho}'_S(t) = &-\int_0^{\Delta t}d\tau\int_t^{t+\Delta t}dt'\Big[\hat{S}'_\alpha(t')\hat{S}'_\beta(t'-\tau)\hat{\rho}'_S(t)-\hat{S}'_\beta(t'-\tau)\hat{\rho}'_S(t)\hat{S}'_\alpha(t')\Big] \\ &+\Big[\hat{\rho}'_S(t)\hat{S}'_\beta(t'-\tau)\hat{S}'_\alpha(t')-\hat{S}'_\alpha(t')\hat{\rho}'_S(t)\hat{S}'_\beta(t'-\tau)\Big].\end{aligned} \tag{B.18}$$

We will make the following assumption [44] about $\hat{S}'_\alpha(t)$ and $\hat{S}'_\beta(t)$:

$$\hat{S}'_{\alpha(\beta)}(t)=e^{iH_st/\hbar}\hat{S}_{\alpha(\beta)}e^{-iH_st/\hbar}=\hat{S}_{\alpha(\beta)}e^{i\omega_{\alpha(\beta)}t}, \tag{B.19}$$

where the $\omega_{\alpha(\beta)}$ is a frequency associated with the system operator $\hat{S}_{\alpha(\beta)}$. Equation (B.18) can thus be rewritten as follows:

$$\Delta\hat{\rho}'_S(t)=-\left[\left(\hat{S}_\alpha\hat{S}_\beta\hat{\rho}'_S(t)-\hat{S}_\beta\hat{\rho}'_S(t)\hat{S}_\alpha\right)w^+ +\left(\hat{\rho}'_S(t)\hat{S}_\beta\hat{S}_\alpha-\hat{S}_\alpha\hat{\rho}'_S(t)\hat{S}_\beta\right)w^-\right]I(\omega_\alpha+\omega_\beta), \tag{B.20}$$

where:

$$w^{+} = \int_{0}^{\Delta t} d\tau e^{-i\omega_\beta \tau}, \tag{B.21}$$

$$w^{-} = \int_{0}^{\Delta t} d\tau e^{i\omega_\beta \tau}, \tag{B.22}$$

$$I(\omega_\alpha + \omega_\beta) = \int_{t}^{t+\Delta t} dt' e^{-i(\omega_\alpha+\omega_\beta)t'}. \tag{B.23}$$

Assuming that the system-reservoir interaction has fast dynamics compared with the dynamics of each one separately, one can write:

$$\Delta t \gg (\omega_\alpha + \omega_\beta)^{-1},$$

which implies that $I(\omega_\alpha+\omega_\beta)$ tends to zero for all ω_α and ω_β values, except for $\omega_\alpha+\omega_\beta = 0$. Then $I(\omega_\alpha + \omega_\beta)$ can be expressed in terms of a Kronecker function $\delta(\omega_\alpha, -\omega_\beta)$ as:

$$I(\omega_\alpha + \omega_\beta) = \Delta t \delta(\omega_\alpha, -\omega_\beta). \tag{B.24}$$

It is thus possible to rewrite Eq. (B.20) as:

$$\frac{\Delta \hat{\rho}'_{RS}}{\Delta t} = -\left[\left(\hat{S}_\alpha \hat{S}_\beta \hat{\rho}'_S(t) - \hat{S}_\beta \hat{\rho}'_S(t) \hat{S}_\alpha\right) w^{+} + \left(\hat{\rho}'_S(t) \hat{S}_\beta \hat{S}_\alpha - \hat{S}_\alpha \hat{\rho}'_S(t) \hat{S}_\beta\right) w^{-}\right] \delta(\omega_\alpha, -\omega_\beta). \tag{B.25}$$

Taking the limit of small Δt, so that $\lim_{\Delta t \to 0} \frac{\Delta \hat{\rho}'_{RS}}{\Delta t} \to \frac{\partial \hat{\rho}'_{RS}}{\partial t}$, and sending Eq. (B.25) back to the Schrodinger picture [44], we are left with:

$$\begin{aligned} \partial_t \hat{\rho}_S(t) = &-\frac{i}{\hbar}\left[\hat{H}_s, \hat{\rho}_S(t)\right] \\ &- \left[\left(\hat{S}_\alpha \hat{S}_\beta \hat{\rho}'_S(t) - \hat{S}_\beta \hat{\rho}_S(t) \hat{S}_\alpha\right) w^{+} + \left(\hat{\rho}_S(t) \hat{S}_\beta \hat{S}_\alpha - \hat{S}_\alpha \hat{\rho}_S(t) \hat{S}_\beta\right) w^{-}\right] \delta(\omega_\alpha, -\omega_\beta). \end{aligned} \tag{B.26}$$

From Eqs. (B.21) and (B.22), we have that w^{+} and w^{-} are complex functions, so they can be written as $w^{\pm} = \mathrm{Re}[w^{\pm}] + i\mathrm{Im}[w^{\pm}]$, where $w^{-} = [w^{+}]^{*}$. These relations combined with the fact that terms where $S_\alpha = S_\beta^\dagger$ satisfy $\delta(\omega_\alpha, -\omega_\beta) = 1$, allow us to rewrite Eq. (B.26) in terms of α only:

$$\begin{aligned} \partial_t \hat{\rho}(t) = &\frac{i}{\hbar}\left[\hat{H}_S, \hat{\rho}_S(t)\right] - i \sum_\alpha \mathrm{Im}[w^{+}] \left[\hat{S}_\alpha \hat{S}_\alpha^\dagger, \hat{\rho}\right] \\ &+ \sum_\alpha 2\mathrm{Re}[w^{+}] \left[\hat{S}_\alpha^\dagger \hat{\rho} \hat{S}_\alpha - \frac{1}{2}\left(\hat{S}_\alpha \hat{S}_\alpha^\dagger \hat{\rho} + \hat{\rho} \hat{S}_\alpha^\dagger \hat{S}_\alpha\right)\right], \end{aligned} \tag{B.27}$$

where the explicit summation symbol over α was reinserted. Defining $\hbar \sum_\alpha w^{+}[\hat{S}_\alpha \hat{S}_\alpha^\dagger, \hat{\rho}] \equiv H_{eff}$ and $2\mathrm{Re}[w^{+}] \equiv k_\alpha$, we can further write:

$$\partial_t \hat{\rho}_S(t) = -\frac{i}{\hbar}[\hat{H}_S + \hat{H}_{eff}, \hat{\rho}_S] + \sum_\alpha k_\alpha \left[\hat{S}_\alpha^\dagger \hat{\rho}_S \hat{S}_\alpha - \frac{1}{2}\left(\hat{S}_\alpha \hat{\rho}_S \hat{S}_\alpha^\dagger + \hat{\rho}_S \hat{S}_\alpha^\dagger \hat{S}_\alpha\right)\right]. \tag{B.28}$$

We now define the last term in Eq. (B.27) as a superoperator (an operator which acts over the density matrix) as:

$$\mathcal{L}[\hat{\rho}_S] = \sum_{\alpha} k_\alpha \left[\hat{S}_\alpha^\dagger \hat{\rho}_S \hat{S}_\alpha - \frac{1}{2} \left(\hat{S}_\alpha \hat{\rho}_S \hat{S}_\alpha^\dagger + \hat{\rho}_S \hat{S}_\alpha^\dagger \hat{S}_\alpha \right) \right],$$

which can be generalized:

$$\mathcal{L}[\hat{\rho}] = \hat{c}\hat{\rho}\hat{c}^\dagger - \frac{1}{2} \left(\hat{c}^\dagger \hat{c}\hat{\rho} + \hat{\rho}\hat{c}^\dagger \hat{c} \right). \tag{B.29}$$

We can put away the real constant k_α without loss of generality. Finally, Eq. (B.28) can be written as:

$$\partial_t \hat{\rho}(t) = -\frac{i}{\hbar}[\hat{H}, \rho] + \mathcal{L}[\hat{\rho}]. \tag{B.30}$$

Equation (B.30) is called a *Master Equation* and $\mathcal{L}[\hat{\rho}]$ is a Liouvillian superoperator acting on the density matrix $\hat{\rho}$ called *Lindbladian*, which accounts for energy shifts and dissipation effects due to the interaction with the reservoir.

C The Python codes in QuTip Toolbox

C.1 The Green tensor

```
from qutip import *
import numpy as np

def Green_Tensor(Gamma,R,k,i,j):
    G = np.add(np.zeros((3,3)),np.multiply(1j,np.zeros((3,3))))
    if (i != j):
        R_ij = np.add(R[i],np.multiply(-1.0,R[j])) #The position vector
        r_ij = np.linalg.norm(R_ij) #The position vector module
        G = (3.0*Gamma/4.0)*((np.exp(1j*k*r_ij))/(((k*r_ij)**3)))*((k*
    r_ij)**2 + 1j*k*r_ij -1)*np.identity(3)-((k*r_ij)**2 + 1j*3*k*r_ij
    -3)*np.tensordot(R_ij,R_ij,axes=0)
    else:
        G = 1j*Gamma/2*np.identity(3)
    return G
```

C.2 The creation and annihilation atomic operators

```
from qutip import *

def Sigmam(N,level,i):
    q_list = [qeye(level)]*N #N identity quantum objects in a subspace
    of the Hilbert space with dimension defined by the "level" variable.
    q_list[i] = sigmam() #It applies the annihilation atomic operator at
    i-th position of q_list
    sigmamN = tensor(q_list) #The tensorial product between the q_list
    elements
    return sigmamN

def Sigmap(N,level,i):
    q_list = [qeye(level)]*N
    q_list[i] = sigmap() #It applies the creation atomic operator at i-
    th position of q_list
    sigmapN = tensor(q_list)
    return sigmapN
```

C.3 The electric field

```
from qutip import *
import numpy as np

```

```
import sigma_plus
import sigma_minus

def E(N,k,n_hat,R,level,signal):
    E = 0
    for i in range(0,N):
        if signal == 'plus':
            E += np.exp(-1j*k*np.dot(n_hat,R[i]))*sigma_minus.Sigmam(N,level,i) #The positive component of the electric field
        else:
            E += np.exp(1j*k*np.dot(n_hat,R[i]))*sigma_plus.Sigmap(N,level,i)   #The negative component of the electric field
    return E
```

C.4 The position vector

```
def position_vector(d,N): #The construction of the atomic position vector for a linear chain of atoms
    R = [[0,0,0]]
    j = 0
    while j < (N-1):
        j = j + 1
        R.append([j*d,0,0])
    print(R)
    return R
```

C.5 The inelastic term Γ^{ij}

```
from qutip import *
import numpy as np
import math

import green_tensor

def f_matrix(Gamma,R,P,k0,N):
  f = np.add(np.zeros((N,N)),np.multiply(1j,np.zeros((N,N))))
 for i in range(0,N):
    for j in range(0,N):
        G_ij = green_tensor.Green_Tensor(Gamma,R,k0,i,j) #The Green tensor
        G_Img = np.imag(G_ij)
        f[i,j]=np.tensordot(np.conj(P[i]),np.tensordot(np.multiply(2,G_Img),P[j],axes=1),axes=1) #The inelastic term
 return f
```

C.6 The elastic term Δ^{ij}

```
from qutip import *
import numpy as np
import math

import green_tensor

def g_matrix(Gamma,R,P,k0,N):
    g = np.add(np.zeros((N,N)),np.multiply(1j,np.zeros((N,N))))
    for i in range(0,N):
        for j in range(0,N):
            G_ij = green_tensor.Green_Tensor(Gamma,R,k0,i,j)
            G_real = np.real(G_ij)
            g[i,j] = np.tensordot(np.conj(P[i]),np.tensordot(G_real,P[j
    ],axes=1),axes=1) #The elastic term
    return g
```

C.7 The Hamiltonian

```
from qutip import *
import numpy as np

import sigma_minus
import sigma_plus
import electric_field

def Hamiltonian(N,R,g,Omega,Delta,k_vec):
    H1,H2,H3 = 0,0,0
    for i in range(0,N):
        SgmP_i = sigma_plus.Sigmap(N,2,i) #The atomic creation operator
    applied on the i-th atom
        SgmM_i = sigma_minus.Sigmam(N,2,i) #The atomic annihilation
    operator applied on the i-th atom
        H1 += -Delta*(SgmP_i*SgmM_i)
        H2 +=  -0.5*Omega*(np.exp(1j*np.dot(k_vec,R[i]))*SgmP_i + np.exp
    (-1j*np.dot(k_vec,R[i]))*SgmM_i)
        for j in range(0,N):
            SgmM_j = sigma_minus.Sigmam(N,2,j) #The atomic annihilation
    operator applied on the j-th atom
            H3 += g[i,j]*SgmP_i*SgmM_j
    H = H1 + H2 + H3 #Hamiltonian
    return H
```

C.8 The Lindbladian

```
from qutip import *

import sigma_minus
```

```
import sigma_plus

def Lindbladian(N,f):
    L = []
    L_parc = 0
    for i in range(0,N):
        SgmM_i = sigma_minus.Sigmam(N,2,i)
        for j in range(0,N):
            SgmP_j = sigma_plus.Sigmap(N,2,j)
            L_parc += f[i,j]*(2*(qutip.spre(SgmM_i)*qutip.spost(SgmP_j))
    - (qutip.spre(SgmP_j*SgmM_i)+qutip.spost(SgmP_j*SgmM_i)))
        L.append(0.5*L_parc) #Lindbladian
    return L
```

C.9 The projector for the single-excitation state

```
from qutip import *

def psi1_projector(N):
    psi1,projector_total= 0,0
    list_state = [basis(2,1)]*N  #A list of N quantum objects
   representing the N ground state atoms
    for i in range(0,N):
        list_state[i] = basis(2,0) #It applies an excitation in the i-th
    atom
        psi1 = (tensor(list_state)).unit() #Normalized tensor product
   between the list_state elements, which consists in the single-
   excitation state
        projector = psi1*psi1.dag() #The projector for the single-
   excitation state
        projector_total += projector #The sum of the single-excitation
   projectors for the N atoms
        list_state[i] = basis(2,1)
        psi1 = 0
    return projector_total
```

C.10 The projector for the two-excitation state

```
from qutip import *

def psi2_projector(N):
    psi2,projector_total = 0,0
    list_state = [basis(2,1)]*N
    for i in range(0,N):
        list_state[i] = basis(2,0)
        j=0
        while(j<i):
```

```
            list_state[j] = basis(2,0)
            psi2 = (tensor(list_state)).unit() #Normalized tensor product between the list_state elements, which consists in the two-excitation state
            projector = psi2*psi2.dag() #The projector for the two-excitation state
            projector_total += projector #The sum of the two-excitation projectors for the N atoms
            j += 1
            list_state[j] = basis(2,1)
            psi2 = 0
        list_state[i] = basis(2,1)
    return projector_total
```

C.11 The projector for the three-excitation state

```
from qutip import *

def psi3_projector(N):
    psi3, projector_total = 0,0
    list_state = [basis(2,1)]*N
    for i in range(0,N):
        list_state[i] = basis(2,0)
        j = 0
        while (j<i):
            list_state[i] = basis(2,0)
            k = 0
            while(k<j):
                list_state[k] = basis(2,0)
                psi3 = (tensor(list_state)).unit() #Normalized tensor product between the list_state elements, which consists in the three-excitation state
                projector = psi3*psi3.dag() #The projector for the three-excitation state
                projector_total += projector #The sum of the three-excitation projectors for the N atoms
                psi3 = 0
                list_state[k] = basis(2,1)
                k += 1
            list_state[j] = basis(2,1)
            j += 1
        list_state[i] = basis(2,1)
    return projector_total
```

C.12 The P_2/P_1^2 plot in terms of Δ/Γ

```
from qutip import *
```

```
2 import numpy as np
3 import matplotlib.pyplot as plt
4 import scipy.linalg as la
5 import h5py
6 import os
7
8 import position_vector
9 import gamma_function
10 import delta_function
11 import hamiltonian
12 import lindbladian
13 import psi1_projector
14 import psi2_projector
15 import plot
16
17 #General Parameters
18
19 Gamma = 1 #The atomic system linewidth
20 N = 2 #The number of atoms
21 level = 2 #Two-level atoms
22 n_hat = [0,1,0] #It defines the direction of the incident laser
23 Omega = 30*Gamma #Rabi frequency
24
25 #Geometry
26
27 k0=2*np.pi
28 k_vec = [0,k0,0] #The wave vector
29 k = np.linalg.norm(k_vec) #The wave vector module
30 d = 0.2/k #The interatomic distance
31 p = [0,0,1] #It defines the polarization direction
32 P = [p]*N #The polarization vector
33 R = position_vector.position_vector(d,N) #The position vector
34
35 #Model
36 vector_model = 1
37 scalar_model = 0
38
39 if vector_model:
40     f = gamma_function.f_matrix(Gamma,R,P,k0,N) #The inelastic term for
    the vector model of light
41     g = delta_function.g_matrix(Gamma,R,P,k0,N) #The elastic term for
    the vector model of light
42
43 if scalar_model:
44     f = gamma_function.gamma_escalar(N,R,k0,Gamma) #The inelastic term
    for the scalar model of light
45     g = delta_function.delta_escalar(N,R,k0,Gamma) #The elastic term for
```

```
    the scalar model of light

c_ops = lindbladian.Lindbladian(N,f) #The Lindbladian

n_exc_1 = psi1_projector.psi1_projector(N) #The projector of the single-
    excitation state
n_exc_2 = psi2_projector.psi2_projector(N) #The projector of the two-
    excitation state
e_ops = [n_exc_1,n_exc_2]
ratio_list = []
count = 0

for Delta in delta_points:
    H = hamiltonian.Hamiltonian(N,R,g,Omega,Delta,k_vec) #The
    Hamiltonian
    result = steadystate(H,c_ops) #The state vector
    n1 = expect(n_exc_1,result) #The population of the single-excitation
    state
    n2 = expect(n_exc_2,result) #The population of the two-excitation
    state
    ratio = n2/(n1**(2)) #The ratio P2/P1^2
    print(ratio)
    ratio_list.append(ratio) #The list of the P2/P1^2 values for each
    Delta
```

C.13 The intensity-intensity correlation function $g^{(2)}(0)$

```
from qutip import *
import numpy as np

import hamiltonian
import electric_field
import sigma_plus
import sigma_minus

def g2_0(N,R,g,Omega,Delta,k_vec,c_ops,k,n_hat,level):
    H = hamiltonian.Hamiltonian(N,R,g,Omega,Delta,k_vec) #The
    Hamiltonian
    result = steadystate(H,c_ops)  #The state vector
    E_p = electric_field.E(N,k,n_hat,R,level,'plus') #The positive
    component of the electric field
    E_m = electric_field.E(N,k,n_hat,R,level,'minus') #The negative
    component of the electric field
    numerator = expect(E_m*E_m*E_p*E_p,result)
    denominator = (expect(E_m*E_p,result))**2
    g2_0 = np.divide(numerator,denominator) #The intensity-intensity
    correlation function
```

```
    return g2_0
```

C.14 The $g^{(2)}(0)$ for a system with two and three atoms

```
from qutip import *
import numpy as np


import position_vector
import gamma_function
import delta_function
import hamiltonian
import lindbladian
import plot
import correlation_functions

#General Parameters

Gamma = 1 #The atomic system linewidth
N = 3 #The number of atoms
level = 2 #Two-level atoms
n_hat = [0,1,0] #It defines the direction of the incident laser

#Geometry

k0=2*np.pi
k_vec = [0,k0,0] #The wave vector
k = np.linalg.norm(k_vec) #The wave vector module
d = 0.2/k0 #The interatomic distance
p = [0,0,1] #It defines the polarization direction
P = [p]*N #The polarization vector
R = position_vector.position_vector(d,N) #The position vector


#Model
vector_model = 1
scalar_model = 0

Omega = 30*Gamma #Rabi frequency

if vector_model:
    f = gamma_function.f_matrix(Gamma,R,P,k0,N) #The inelastic term for
    the vector model of light
    g = delta_function.g_matrix(Gamma,R,P,k0,N) #The elastic term for
    the vector model of light

if scalar_model:
```

```
    f = gamma_function.gamma_escalar(N,R,k0,Gamma) #The inelastic term
   for the scalar model of light
    g = delta_function.delta_escalar(N,R,k0,Gamma) #The elastic term for
    the scalar model of light

c_ops = lindbladian.Lindbladian(N,f) #The Lindbladian

if N == 3:
    g2_list = []
    count = 0
    for Delta in points:
        H = hamiltonian.Hamiltonian(N,R,g,Omega,Delta,k_vec) #The
   Hamiltonian
        result = steadystate(H,c_ops) #The state vector
        g2 = correlation_functions.g2_0(N,R,g,Omega,Delta,k_vec,c_ops,k,
   n_hat,level) #The intensity-intensity correlation function
        g2_list.append(g2) #The list of the intensity-intensity
   correlation function values for each Delta
        count += 1
        print(count)

if N == 2:
    g2_list = []
    count = 0
    for Delta in points:
        H = hamiltonian.Hamiltonian(N,R,g,Omega,Delta,k_vec)
        result = steadystate(H,c_ops)
        g2 = correlation_functions.g2_0(N,R,g,Omega,Delta,k_vec,c_ops,k,
   n_hat,level)
        g2_list.append(g2)
        count += 1
        print(count)
```

C.15 The Populations

```
from qutip import *
import numpy as np
import h5py
import os

import position_vector
import gamma_function
import delta_function
import hamiltonian
import lindbladian
import psi1_projector
import psi2_projector
```

```
13 import psi3_projector
14
15
16 #General Parameters
17
18 Gamma = 1 #The atomic system linewidth
19 N = 2 #The number of atoms
20 level = 2 #Two-level atoms
21 n_hat = [0,1,0] #It defines the direction of the incident laser
22
23 #Geometry
24
25 k0=2*np.pi
26 k_vec = [0,k0,0] #The wave vector
27 k = np.linalg.norm(k_vec) #The wave vector module
28 d = 0.2/k #The interatomic distance
29 p = [0,0,1] #It defines the polarization direction
30 P = [p]*N #The polarization vector
31 R = position_vector.position_vector(d,N) #The position vector
32
33 Omega = 30*Gamma #Rabi frequency
34 f = gamma_function.f_matrix(Gamma,R,P,k0,N) #The inelastic term for the
    vector model of light
35 g = delta_function.g_matrix(Gamma,R,P,k0,N) #The elastic term for the
    vector model of light
36 c_ops = lindbladian.Lindbladian(N,f) #The Lindbladian
37
38 if N == 3:
39
40     n_exc_1 = psi1_projector.psi1_projector(N) #The projector of the
    single-excitation state
41     n_exc_2 = psi2_projector.psi2_projector(N) #The projector of the two
    -excitation state
42     n_exc_3 = psi3_projector.psi3_projector(N) #The projector of the
    three-excitation state
43     e_ops = [n_exc_1,n_exc_2,n_exc_3]
44     n1_list = []
45     n2_list = []
46     n3_list = []
47     count = 0
48
49     for Delta in points:
50         H = hamiltonian.Hamiltonian(N,R,g,Omega,Delta,k_vec)
51         result = steadystate(H,c_ops)
52         n1 = expect(e_ops[0],result) #The population of the single-
    excitation state
53         n2 = expect(e_ops[1],result) #The population of the two-
```

```
    excitation state
54          n3 = expect(e_ops[2],result) #The population of the three-
    excitation state
55          n1_list.append(n1) #The n1 values list for each Delta
56          n2_list.append(n2) #The n2 values list for each Delta
57          n3_list.append(n3) #The n3 values list for each Delta
58          count += 1
59          print(count)
60 if N == 2:
61
62      n_exc_1 = psi1_projector.psi1_projector(N)
63      n_exc_2 = psi2_projector.psi2_projector(N)
64      e_ops = [n_exc_1,n_exc_2]
65      n1_list = []
66      n2_list = []
67      count = 0
68
69      for Delta in points:
70          H = hamiltonian.Hamiltonian(N,R,g,Omega,Delta,k_vec)
71          result = steadystate(H,c_ops)
72          n1 = expect(e_ops[0],result)
73          n2 = expect(e_ops[1],result)
74          n1_list.append(n1)
75          n2_list.append(n2)
76          count += 1
77          print(count)
```

C.16 The fluorescence spectrum

```
1  from qutip import *
2  import numpy as np
3  import h5py
4  import os
5
6  import hamiltonian
7  import lindbladian
8  import position_vector
9  import delta_function
10 import gamma_function
11 import filename_generator
12 import sigma_plus
13 import sigma_minus
14 import electric_field
15
16 #General Parameters
17
18 Gamma = 1 #The atomic system linewidth
```

```
Gamma_s = Gamma #The sensor linewidth
epsilon = 10**(-1) #The atomic system-sensor coupling constant
Delta = 0 #The detuning between the incident laser energy and the atomic
    transition energy
N = 2 #The number of atoms
S = 2 #The number of sensor
Omega = 30*Gamma #Rabi frequency
level = 2 #Two-level atoms
n_hat = [0,1,0] #It defines the direction of the incident laser
k0=2*np.pi
k_vec = [0,k0,0] #The wave vector
k = np.linalg.norm(k_vec) #The wave vector module
d = 0.2/k  #The interatomic distance
i,j = 0,0

scalar_model = 0
vector_model = 1
sensor_method = 1
spectrum = 0

ksiP_list = []
ksiM_list = []
P_list = []
P_norm_list = []
H_s,L_s = 0,[]

#Parameters of the atomic system
R = position_vector.position_vector(d,N) #The position vector
p = [0,0,1] #It defines the polarization direction
P = [p]*N #The polarization vector

#Models
if vector_model:
    g = delta_function.g_matrix(Gamma,R,P,k0,N) #The inelastic term for
    the vector model of light
    f = gamma_function.f_matrix(Gamma,R,P,k0,N) #The elastic term for
    the vector model of light

if scalar_model:
    g = delta_function.delta_escalar(N,R,k0,Gamma) #The inelastic term
    for the scalar model of light
    f = gamma_function.gamma_escalar(N,R,k0,Gamma) #The elastic term for
    the scalar model of light

#Parameter for the populations
F = N + S #The total number of elements (atoms + sensor)

```

```
61 if sensor_method:
62     H_a = hamiltonian.Hamiltonian_gen(N,R,g,Omega,Delta,k_vec,level,F,S)
       #The atomic Hamiltonian
63     L_a = lindbladian.Lindbladian_gen(N,f,F,level,S) #The atomic
       Lindbladian
64     L_s = lindbladian.Lindbladian_Sensors(N,F,level,Gamma_s,S) #The
       sensor Lindbladian
65     L = L_a + L_s #The atomic system-sensor Lindbladian
66     if spectrum:
67         omega_1,omega_2 = 0,0
68         omega_sensor_list = [omega_1,omega_2] #The frequencies of each
       sensor
69         H_s = hamiltonian.Hamiltonian_Sensors(N,k,n_hat,R,level,F,
       omega_sensor_list,epsilon) #The sensor Hamiltonian
70         H = H_a + H_s  #The atomic system-sensor Hamiltonian
71         E_m = electric_field.E_gen(N,level,F,'minus',n_hat,R,k) #The
       negative component of the electric field
72         E_p = electric_field.E_gen(N,level,F,'plus',n_hat,R,k)  #The
       positive component of the electric field
73         S = spectrum_ss(H,omega_list,L,E_m,E_p) #The fluorescence
       spectrum
74         y_list = S
75     else:
76         for i in range(N,F):
77             ksiP_i = sigma_plus.Sigmap_gen(level,F,i) #The sensor
       creation operator
78             ksiM_i = sigma_minus.Sigmam_gen(level,F,i) #The sensor
       annihilation operator
79             ksiP_list.append(ksiP_i)
80             ksiM_list.append(ksiM_i)
81         for omega in omega_list:
82             print(omega)
83             omega_sensor_list = [omega]*S
84             H_s = hamiltonian.Hamiltonian_Sensors(N,k,n_hat,R,level,F,
       omega_sensor_list,epsilon)
85             H = H_a + H_s
86             result = steadystate(H,L) #The state vector
87             P_i = expect(ksiP_list[0]*ksiM_list[0] + ksiP_list[1]*
       ksiM_list[1],result) #The Population measured by the sensor
88             P_list.append(P_i) #The list of Population values for each
       omega values
89         y_list = P_list
90 else:
91     H = hamiltonian.Hamiltonian(N,R,g,Omega,Delta,k_vec)
92     L = lindbladian.Lindbladian(N,f)
93     E_m = electric_field.E(N,k,n_hat,R,level,'minus')
94     E_p = electric_field.E(N,k,n_hat,R,level,'plus')
```

```
95      S = spectrum_ss(H,omega_list,L,E_m,E_p)
96      y_list = S
```

C.17 The intensity-intensity correlation function for the sensor method $g_{\Gamma}^{(2)}(\omega_1, \omega_2)$ and the Cauchy-Schwarz inequality

```
1  from qutip import *
2  import numpy as np
3  import h5py
4  import os
5
6  import correlation_functions
7  import hamiltonian
8  import lindbladian
9  import position_vector
10 import delta_function
11 import gamma_function
12 import filename_generator
13
14 #General Parameters
15
16 Gamma = 1 #The atomic system linewidth
17 Gamma_s = Gamma #The sensor linewidth
18 epsilon = 10**(-1) #The atomic system-sensor coupling constant
19 Delta = 0 #The detuning between the incident laser energy and the atomic
       transition energy
20 N = 2 #The number of atoms
21 S = 2 #The number of sensor
22 Omega = 30*Gamma #Rabi frequency
23 level = 2 #Two-level atoms
24 n_hat = [0,1,0] #It defines the direction of the incident laser
25 k0=2*np.pi
26 k_vec = [0,k0,0] #The wave vector
27 k = np.linalg.norm(k_vec) #The wave vector module
28 d = 0.2/k #The interatomic distance
29 i,j = 0,0
30
31 scalar_model = 0
32 vector_model = 1
33
34 #Parameters of the atomic system
35 R = position_vector.position_vector(d,N) #The position vector
36 p = [0,0,1] #It defines the polarization direction
37 P = [p]*N #The polarization vector
38
39 if vector_model:
```

```
40      g = delta_function.g_matrix(Gamma,R,P,k0,N) #The inelastic term for
    the vector model of light
41      f = gamma_function.f_matrix(Gamma,R,P,k0,N) #The elastic term for
    the vector model of light
42
43  if scalar_model:
44      g = delta_function.delta_escalar(N,R,k0,Gamma) #The inelastic term
    for the scalar model of light
45      f = gamma_function.gamma_escalar(N,R,k0,Gamma) #The elastic term for
     the scalar model of light
46
47  #Parameter for g_12
48  F = N + S #The total number of elements (atoms + sensor)
49
50
51  #Atomic system
52  H_a = hamiltonian.Hamiltonian_gen(N,R,g,Omega,Delta,k_vec,level,F,S)
    Tthe atomic Hamiltonian
53  L_a = lindbladian.Lindbladian_gen(N,f,F,level,S) #The atomic Lindbladian
54
55  #List and Matrix
56  g_12_Matrix = np.zeros((omega_points,omega_points))
57  g_11_Matrix = np.zeros((omega_points,omega_points))
58  g_22_Matrix = np.zeros((omega_points,omega_points))
59  R_cs_Matrix = np.zeros((omega_points,omega_points))
60  num_12_list = []
61  den_12_list = []
62
63  #Sensors
64  #The sensor method for all frequencies combination
65  for omega_1 in omega_list:
66      for omega_2 in omega_list:
67          print(omega_1,omega_2)
68          omega_sensor_list = [omega_1,omega_2]
69          H_s_12 = hamiltonian.Hamiltonian_Sensors(N,k,n_hat,R,level,F,
    omega_sensor_list,epsilon) #The sensor Hamiltonian
70          L_s_12 = lindbladian.Lindbladian_Sensors(N,F,level,Gamma_s,S)
                #The sensor Lindbladian
71          H_12 = H_a + H_s_12  #The atomic system-sensor Hamiltonian
72          L_12 = L_a + L_s_12  #The atomic system-sensor Lindbladian
73          result_12 = steadystate(H_12, L_12) #The atomic system-sensor
    vector state
74  #The sensor method for omega_2 = omega_1
75          omega_sensor_list = [omega_1,omega_1]
76          H_s_11 = hamiltonian.Hamiltonian_Sensors(N,k,n_hat,R,level,F,
    omega_sensor_list,epsilon)
77          L_s_11 = lindbladian.Lindbladian_Sensors(N,F,level,Gamma_s,S)
```

```
78          H_11 = H_a + H_s_11
79          L_11 = L_a + L_s_11
80          result_11 = steadystate(H_11,L_11,tol = atol)
81 #The sensor method for omega_1 = omega_2
82          omega_sensor_list = [omega_2,omega_2]
83          H_s_22 = hamiltonian.Hamiltonian_Sensors(N,k,n_hat,R,level,F,
       omega_sensor_list,epsilon)
84          L_s_22 = lindbladian.Lindbladian_Sensors(N,F,level,Gamma_s,S)
85          H_22 = H_a + H_s_22
86          L_22 = L_a + L_s_22
87          result_22 = steadystate(H_22,L_22,tol = atol)
88
89          #Correlation Functions
90          g_12,num_12,den_12 = correlation_functions.g2_sensor(H_12,L_12,
       atol,N,F,level) #The intensity-intensity correlation function for
       different frequencies
91          g_11,num_11,den_11 = correlation_functions.g2_sensor(H_11,L_11,
       atol,N,F,level) #The intensity-intensity correlation function for
       omega_2 = omega_1
92          g_22,num_22,den_22 = correlation_functions.g2_sensor(H_22,L_22,
       atol,N,F,level) #The intensity-intensity correlation function for
       omega_1 = omega_2
93
94          R_cs_i = (g_12**2)/(g_11*g_22) #The R term in Cauchy-Schwarz
       inequality for each frequency combination
95
96          g_12_Matrix[i,j] = g_12 #The matrix of the g_12 values
97          g_11_Matrix[i,j] = g_11 #The matrix of the g_11 values
98          g_22_Matrix[i,j] = g_22 #The matrix of the g_22 values
99          R_cs_Matrix[i,j] = R_cs_i #The matrix of the R_cs_i values
100
101         j += 1
102     j = 0
103     i += 1
```

C.18 Bell inequality

```
1  from qutip import *
2  import numpy as np
3  import h5py
4  import os
5
6  import hamiltonian
7  import lindbladian
8  import position_vector
9  import delta_function
10 import gamma_function
```

```
import sigma_plus
import sigma_minus

#General Parameters

Gamma = 1 #The atomic system linewidth
Gamma_s = Gamma #The sensor linewidth
epsilon = 10**(-1)  #The atomic system-sensor coupling constant
Delta = 0 #The detuning between the incident laser energy and the atomic
    transition energy
N = 2 #The number of atoms
S = 2 #The number of sensor
Omega = 30*Gamma #Rabi frequency
level = 2 #Two-level atoms
n_hat = [0,1,0] #It defines the direction of the incident laser
k0=2*np.pi
k_vec = [0,k0,0] #The wave vector
k = np.linalg.norm(k_vec) #The wave vector module
d = 0.2/k #The interatomic distance
i,j = 0,0
vector_model = 1
scalar_model = 0

#Parameters of the atomic system
R = position_vector.position_vector(d,N) #The position vector
p = [0,0,1] #It defines the polarization direction
P = [p]*N #The polarization vector

if vector_model:
    g = delta_function.g_matrix(Gamma,R,P,k0,N) #The inelastic term for
    the vector model of light
    f = gamma_function.f_matrix(Gamma,R,P,k0,N) #The elastic term for
    the vector model of light

if scalar_model:
    g = delta_function.delta_escalar(N,R,k0,Gamma) #The inelastic term
    for the scalar model of light
    f = gamma_function.gamma_escalar(N,R,k0,Gamma) #The elastic term for
    the scalar model of light

#Parameter for g_12
F = N + S #The total number of elements (atoms + sensor)

#Lists and Matrix
ksiM_list = []
ksiP_list = []
B_Matrix = np.zeros((omega_points,omega_points))
```

```
53
54 #Atomic system
55 H_a = hamiltonian.Hamiltonian_gen(N,R,g,Omega,Delta,k_vec,level,F,S) #
   The atomic Hamiltonian
56 L_a = lindbladian.Lindbladian_gen(N,f,F,level,S) #The atomic Lindbladian
57
58 for k in range(N,F):
59     ksiP_i = sigma_plus.Sigmap_gen(level,F,k) #The sensor creation
   operator
60     ksiM_i = sigma_minus.Sigmam_gen(level,F,k) #The sensor annihilation
   operator
61     ksiP_list.append(ksiP_i)
62     ksiM_list.append(ksiM_i)
63
64 for omega_1 in omega_list:
65     for omega_2 in omega_list:
66
67         print(omega_1,omega_2)
68
69         #The Bell inequality element B_1111
70         omega_sensor_list = [omega_1,omega_1]
71         H_s_11 = hamiltonian.Hamiltonian_Sensors(N,k,n_hat,R,level,F,
   omega_sensor_list,epsilon) #The sensor Hamiltonian
72         L_s_11 = lindbladian.Lindbladian_Sensors(N,F,level,Gamma_s,S) #
   The sensor Lindbladian
73         H_11 = H_a + H_s_11  #The atomic system-sensor Hamiltonian
74         L_11 = L_a + L_s_11  #The atomic system-sensor Lindbladian
75         result_11 = steadystate(H_11,L_11) #The atomic system-sensor
   vector state
76         B_1111 = expect(ksiP_list[0]*ksiP_list[1]*ksiM_list[1]*ksiM_list
   [0],result_11) #The corresponding Bell inequality element
77
78         #The Bell inequality element B_2222
79         omega_sensor_list = [omega_2,omega_2]
80         H_s_22 = hamiltonian.Hamiltonian_Sensors(N,k,n_hat,R,level,F,
   omega_sensor_list,epsilon)
81         L_s_22 = lindbladian.Lindbladian_Sensors(N,F,level,Gamma_s,S)
82         H_22 = H_a + H_s_22
83         L_22 = L_a + L_s_22
84         result_22 = steadystate(H_22,L_22,tol = atol)
85         B_2222 = expect(ksiP_list[0]*ksiP_list[1]*ksiM_list[1]*ksiM_list
   [0],result_22)
86
87         #The Bell inequality elements B_1221, B_1122, B_2211
88         omega_sensor_list = [omega_1,omega_2]
89         H_s_12 = hamiltonian.Hamiltonian_Sensors(N,k,n_hat,R,level,F,
   omega_sensor_list,epsilon)
```

```
90          L_s_12 = lindbladian.Lindbladian_Sensors(N,F,level,Gamma_s,S)
91          H_12 = H_a + H_s_12
92          L_12 = L_a + L_s_12
93          result_12 = steadystate(H_12,L_12,tol = atol)
94          B_1221 = expect(ksiP_list[0]*ksiP_list[1]*ksiM_list[1]*ksiM_list
    [0],result_12)
95          B_1122 = expect(ksiP_list[0]*ksiP_list[0]*ksiM_list[1]*ksiM_list
    [1],result_12)
96          B_2211 = expect(ksiP_list[1]*ksiP_list[1]*ksiM_list[0]*ksiM_list
    [0],result_12)
97
98          B_i = np.sqrt(2)*np.abs((B_1111 + B_2222 -4*B_1221 - B_1122 -
    B_2211)/(B_1111 + B_2222 + 2*B_1221)) #The B term of the Bell
    inequality for each frequency combination
99          print(B_i)
100         B_Matrix[i,j] = B_i #The matrix of B_i values
101         j += 1
102     j = 0
103     i += 1
```